

Cenozoic range-front faulting and development of the Transantarctic Mountains near Cape Surprise, Antarctica: Thermochronologic and geomorphologic constraints

Scott R. Miller,¹ Paul G. Fitzgerald,¹ and Suzanne L. Baldwin¹

Received 4 February 2009; revised 5 August 2009; accepted 22 September 2009; published 28 January 2010.

[1] The Transantarctic Mountains (TAM) define the western flank of the West Antarctic rift system. Cape Surprise, near the Shackleton Glacier in the central TAM, is the only location along the range's >3500 km length where upper Paleozoic Beacon Supergroup strata are down-faulted to near sea level. Previous studies have inferred a range front master normal fault accommodates extension and rock uplift across the TAM front in this region. The history of rock uplift is debated, suggested as early as Mesozoic, typically Cenozoic, or even Pliocene or younger. Structural observations, apatite fission track (AFT) thermochronology, and geomorphologic mapping undertaken within the TAM front east of the Shackleton Glacier indicate extension, faulting, and denudation was mostly late Eocene–late Oligocene and likely into the early Miocene. An exhumed AFT partial annealing zone is found at the coast and traced >50 km inland. The base of that exhumed partial annealing zone indicates denudation accelerated at ~40 Ma near the coast and at 30–35 Ma on the inland side of the TAM front. Vertically offset AFT isochrones across the TAM front reveal a step-faulted architecture rather than a single master fault. The cumulative vertical offset of the 55 Ma isochrone is 2.3–2.7 km, compared to 2.4–2.6 km offset of Beacon strata, indicating that all significant normal faulting is Cenozoic, and not related to Mesozoic extension within the West Antarctic rift system. Denudation from <26 Ma to ~14 Ma produced a locally preserved erosion surface within the TAM front. Erosion surface remnants indicate the TAM front has undergone minimal internal deformation and only 290–790 m of surface uplift along offshore faults since the middle Miocene. **Citation:** Miller, S. R., P. G. Fitzgerald, and S. L. Baldwin (2010), Cenozoic range-front faulting and development of the Transantarctic Mountains near Cape Surprise, Antarctica: Thermochronologic and

geomorphologic constraints, *Tectonics*, 29, TC1003, doi:10.1029/2009TC002457.

1. Introduction

[2] With a total length of ~3500 km and peak elevations exceeding 4000 m, the Transantarctic Mountains (TAM) are the highest and among the longest intracontinental extensional mountain ranges in the world. The TAM have an influential role in the Antarctic environment, including effects on East Antarctic ice sheet dynamics [Huybrechts, 1993; Kerr and Huybrechts, 1999], yet their origin remains debated and poorly understood [see Fitzgerald, 2002; Bialas *et al.*, 2007]. This mountain range formed along the edge of the East Antarctic craton at its boundary with the Mesozoic to recent West Antarctic rift system (WARS; Figure 1) [e.g., Davey and Brancolini, 1995]. Given the TAM's general structure as a rift flank uplift, many proposed explanations link uplift of the mountain range to WARS extension [Fitzgerald *et al.*, 1986; Stern and ten Brink, 1989; van der Beek *et al.*, 1994; Busetti *et al.*, 1999; van Wijk *et al.*, 2008]. Other authors have suggested that strike-slip faulting rather than normal faulting along the range front permitted uplift of isostatically uncompensated crust [ten Brink *et al.*, 1997]. More recent numerical models and studies of crustal thickness in the TAM have inferred the mountain range is the elevated margin of a rifted, collapsed Mesozoic continental plateau and thus largely the remnant of preexisting high topography and thick crust [Studinger *et al.*, 2004; Karner *et al.*, 2005; Bialas *et al.*, 2007]. Finally, flexural uplift models suggest ~2 km of rock uplift and significant peak uplift may be an isostatic response to Cenozoic glacial erosion and thus not directly tied to rifting [Stern *et al.*, 2005].

[3] Because the WARS and the sedimentary record of mountain building are largely covered by the Ross Sea, the Ross Ice Shelf, and the West Antarctic ice sheet, low-temperature thermochronology applied to the TAM has constrained the cooling history and denudation record of the TAM, and indirectly the tectonic history of the WARS. A series of studies at different geographic locations along the mountain range have applied apatite fission track (AFT) [e.g., Gleadow and Fitzgerald, 1987; Fitzgerald and Gleadow, 1988; Fitzgerald, 1992; Stump and Fitzgerald, 1992; Fitzgerald, 1994; Redfield, 1994; Balestrieri *et al.*, 1997; Fitzgerald and Stump, 1997; Lisker, 2002; Lisker *et al.*, 2006; Fitzgerald and Baldwin, 2007; Storti *et al.*, 2008],

¹Department of Earth Sciences, Syracuse University, Syracuse, New York, USA.

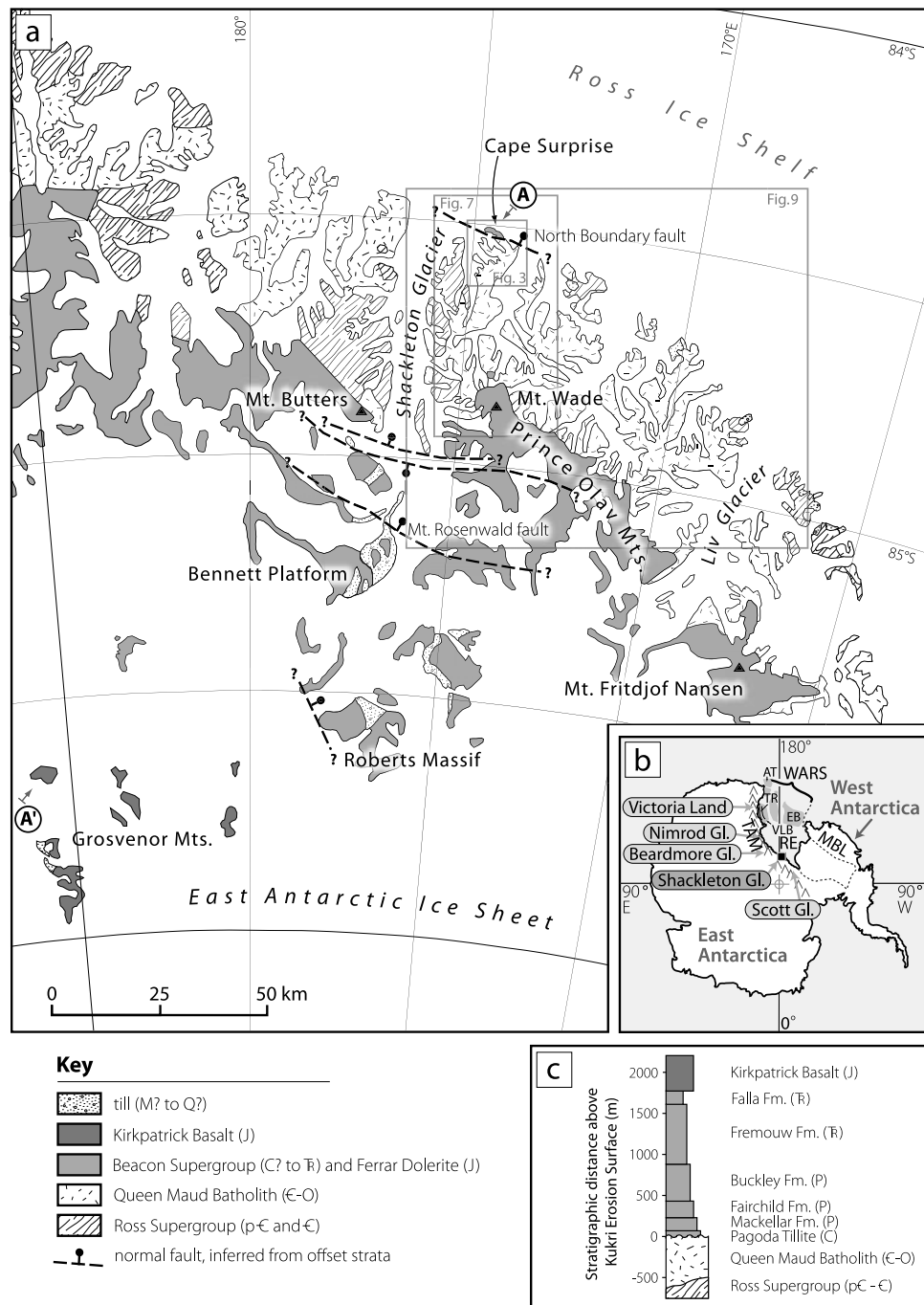


Figure 1. (a) Geological map of the study area, showing major normal faults observed in the field by offset strata [after La Prade, 1969; McGregor and Wade, 1969]. Locations of Figures 3, 7, and 9, and cross section A-A' in Figure 12 are marked. (b) Inset map of Antarctica showing location of study area, near Shackleton Glacier, as well as sites of other studies and features mentioned in the text. AT, Adare Trough; EB, Eastern Basin; MBL, Marie Byrd Land; RE, Ross Embayment; TAM, Transantarctic Mountains; TR, Terror Rift; VLB, Victoria Land Basin; WARS, West Antarctic rift system. (c) Simplified stratigraphic column of study area [after La Prade, 1969; Collinson and Elliot, 1984]. Ferrar Dolerite sills are not shown.

(U-Th)/He [Fitzgerald et al., 2006], and $^{40}\text{Ar}/^{39}\text{Ar}$ thermochronology [Baldwin et al., 1999; Mortimer et al., 2002]. These studies document crustal cooling during the Jurassic (165–150 Ma) [Fitzgerald and Baldwin, 2007], the Early and Late Cretaceous (125–110 Ma and 100–85 Ma) [Stump and Fitzgerald, 1992; Fitzgerald, 1994; Redfield, 1994; Balestrieri et al., 1997; Fitzgerald and Stump, 1997], and the Cenozoic [Gleadow and Fitzgerald, 1987; Fitzgerald and Gleadow, 1988; Fitzgerald, 1992, 1994; Fitzgerald and Stump, 1997; Rossetti et al., 2003]. Cenozoic cooling was initiated from 55 to 45 Ma and associated with 4–9 km of denudation along the mountain front, compared to 1–2 km during the Cretaceous. Yet, no simple relationship exists between Cenozoic denudation and Cenozoic extension in the WARS, most of which occurred from 43 to 26 Ma [Cande et al., 2000; Cande and Stock, 2006; Davey et al., 2006] and from 17 Ma onward in the Victoria Land Basin [Fielding et al., 2008]. One explanation largely decouples tectonics and denudation, suggesting that Cretaceous extension may have caused faulting and generated relief in the TAM but that denudation of the rift flank did not become rapid until climate changed and/or barriers to sediment transport were removed in the Eocene [Studinger et al., 2004; Karner et al., 2005]. However, a key piece of evidence for testing models of TAM formation, namely, the timing of actual rift flank faulting, is rare. This fault zone along the rift margin of the range is termed the TAM front [Barrett, 1981]. Few constraints exist on faulting across the TAM front except for offset rock of Paleozoic and Jurassic age in the central TAM and southern Victoria Land [Gunn and Warren, 1962; Barrett, 1965; Wilson, 1992, 1993], offset Cenozoic AFT isochrones in southern Victoria Land and the Beardmore Glacier area [Fitzgerald, 1992, 1994], and dated pseudotachylites in northern Victoria Land [Di Vincenzo et al., 2004].

[4] In contrast to nearly everywhere else in the TAM, normal faults in the mountain front at Cape Surprise ($84^{\circ}31'S$, $174^{\circ}25'W$), near the Shackleton Glacier, can be readily observed and their displacements relatively well constrained (Figure 1). Cape Surprise is the only place along the entire length of the mountain range where Paleozoic strata are down-faulted from their typically high elevations near the range crest to near sea level [Barrett, 1965]. The occurrence of Beacon strata at this location was originally interpreted as evidence that the TAM front consisted of a single, large-magnitude normal fault, named the so-called “North Boundary fault,” with 3.1–5.2 km of throw [Barrett, 1965; McGregor, 1965; La Prade, 1969]. Models for the uplift of the TAM that require a lithosphere penetrating fault between East and West Antarctica have used the North Boundary fault as the type example [Stern and ten Brink, 1989; ten Brink et al., 1997]. Nevertheless, little is known in detail about the structure of the Cape Surprise region, when the TAM front faults there were active, or its history of landscape evolution and denudation tied to mountain building and climate change.

[5] This study was undertaken to determine the timing and rate of denudation and deformation across the TAM front, to assess if deformation was accommodated by one

large fault (i.e., the North Boundary fault) or a number of smaller faults. Results of AFT thermochronology from 54 samples, including a structural transect and a series of five near-vertical sampling profiles along with geologic constraints, indicate the age and magnitude of fault displacement in the TAM front. Identification of relict erosion surfaces between the Shackleton and Liv glaciers (Figure 1a) places additional limits on the pattern and history of late Cenozoic faulting and surface uplift in the TAM front.

2. Tectonic Background of the West Antarctic Rift System

[6] Extension in the WARS (Figure 1b) began in the Jurassic, associated with widespread tholeiitic magmatism at \sim 180 Ma [Elliot, 1992; Elliot and Fleming, 2004] and dike emplacement along the TAM [Wilson, 1993]. Since rifting began, there has been \sim 400 km of extension between Marie Byrd Land in West Antarctica and the East Antarctic craton [Fitzgerald et al., 1986; DiVenere et al., 1994; Lawver and Gahagan, 1994; Davey and Brancolini, 1995; Lawver and Gahagan, 1995]. Most of this extension occurred 105–85 Ma [Lawver and Gahagan, 1994, 1995] producing four major north–south trending elongate basins in the Ross Sea [Cooper et al., 1991]. Initial extension, probably focused in the eastern part of the rift system [Luyendyk et al., 2003], was accommodated largely along low-angle normal faults [Fitzgerald and Baldwin, 1997; Luyendyk et al., 2001; Siddoway et al., 2004]. This was followed by up to 150–170 km of extension between 43 and 26 Ma [Cande et al., 2000; Cande and Stock, 2006; Davey et al., 2006] focused in the western Ross Sea [Decesari et al., 2007a, 2007b]. Renewed extension within the Terror Rift in the west began in the Miocene (\sim 17 Ma) [Fielding et al., 2008] and is ongoing, as indicated by active volcanism and neotectonic faulting [Jones, 1997]. Although the role of strike-slip faulting in Cenozoic extension within the western Ross Sea is debated [see Storti et al., 2008], strike-slip faulting in northern Victoria Land likely began between 50 and 40 Ma and continued at least through 34 Ma [Di Vincenzo et al., 2004; Rossetti et al., 2006].

3. Geology of the Shackleton Glacier Area

[7] Between the Shackleton and Liv glaciers the TAM have an exposed width of \sim 200 km (Figure 1). The mountain range is characterized by a well-defined northern margin along the Ross Ice Shelf, contrasting with a higher elevation, southern or inboard margin consisting of mesas and nunataks onlapped by the East Antarctic ice sheet (Figure 2). The northern part coincides with the TAM front and consists of a relatively low-relief piedmont \sim 35 km wide, with peaks generally $<$ 1600 m in elevation. This piedmont abuts the prominent frontal escarpment of the Prince Olav Mountains, which reach elevations $>$ 4000 m. Bedrock ridges in the piedmont trend mostly north–south and expose Cambro-Ordovician Queen Maud Batholith granitoids and late Precambrian to Cambro-Ordovician Ross Supergroup metamorphic rocks (Figure 1) [McGregor,

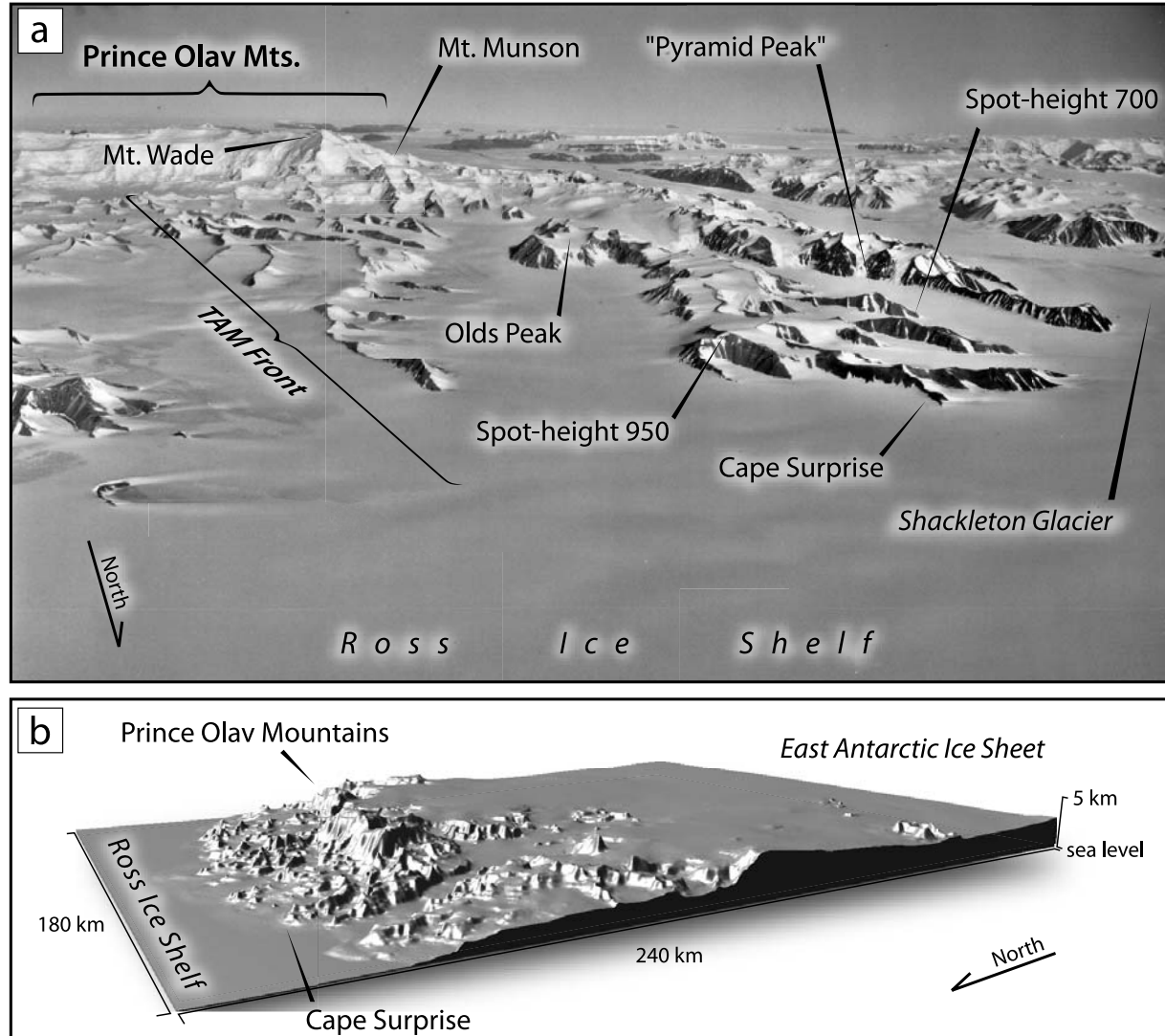


Figure 2. (a) Aerial photograph of the study area (U.S. Navy photograph, TMA 938, 75, F-33). Mount Wade (4084 m) is the highest peak. (b) Digital elevation model (DEM) perspective of the study area, viewed from the northwest, showing the dramatic contrast in elevations between the low-lying basement foothills along the Ross Ice Shelf, the high-relief frontal escarpment of the Prince Olav Mountains, and the Beacon-capped peaks and plateaus farther south. Scene created from the 200 m resolution Radarsat Antarctic Mapping Project (RAMP) DEM [Liu et al., 2001]. Vertical exaggeration is 2×.

1965; Borg, 1983; Stump, 1995] formed during the Ross Orogeny in a continental arc setting [e.g., Stump, 1995; Goode et al., 2004a, 2004b; Paulsen et al., 2004]. The Kukri erosion surface, a regionally extensive Devonian or older unconformity, truncates the basement [Isbell, 1999]. In the Prince Olav Mountains and at Cape Surprise, Carboniferous(?)–Permian Beacon Supergroup strata, intruded by Jurassic Ferrar Dolerite sills and dikes, unconformably overlie the Kukri erosion surface [Barrett, 1965; La Prade, 1969; Barrett, 1991]. These units generally dip southward, gently at Mount Munson and the Prince Olav Mountains (2° – 6° SW) but steeper at Cape Surprise (18° – 35° SW) likely due to fault block tilting. South of Cape Surprise, a

80 m thick dolerite sill intrudes basement rocks \geq 760 m below the Kukri erosion surface and dips \sim 25°SW [Miller et al., 2001]. We infer this basement sill is parallel to the Kukri erosion surface, as commonly observed elsewhere in the TAM [e.g., Hamilton et al., 1965; Fitzgerald, 1992]. Estimates of Beacon Supergroup thickness in the study area range from >1430 m [La Prade, 1970] to 1720–1910 m [Collinson and Elliot, 1984]. The Ferrar Dolerite is 1220–1350 m thick [La Prade, 1969; D. Elliot, personal communication, 2009]. The stratigraphically highest unit, the Jurassic Kirkpatrick Basalt crops out in the southernmost part of the region in the Grosvenor Mountains where it is 430–610 m thick [La Prade, 1969; Barrett et al., 1986].

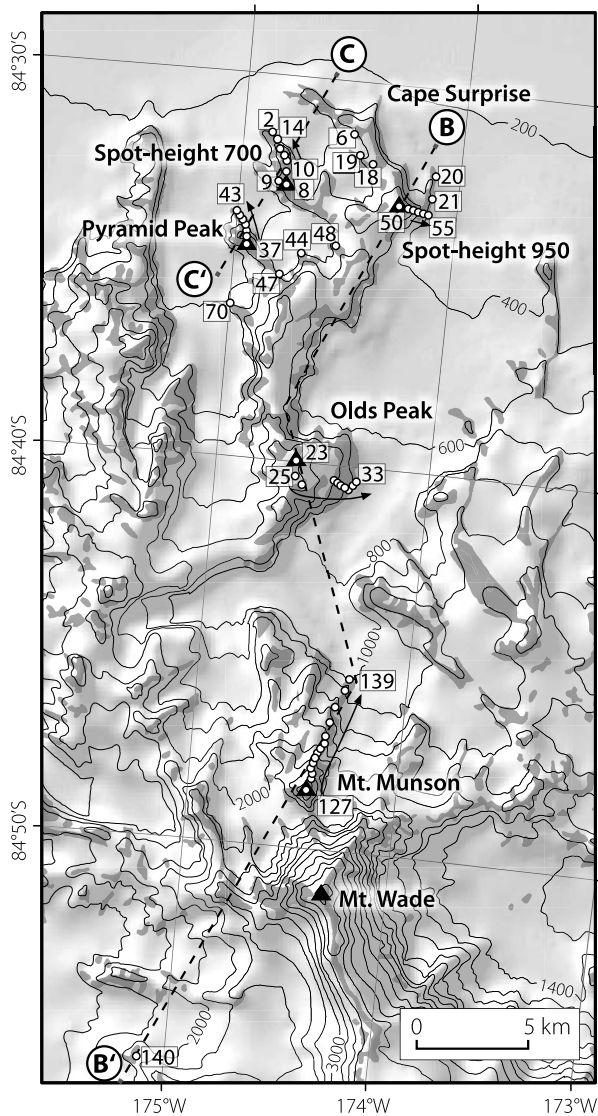


Figure 3. Map showing AFT sample locations (circles), rock outcrops (gray polygons), and select peaks (triangles). Sample numbers, omitting SG prefix, are shown in boxes. Thin dashed lines show locations of the cross section in Figure 8b. Contour interval is 200 m.

These basalts appear to have been confined to a rift, so their lateral extent is unclear [Elliot and Fleming, 2004]. The total thickness of sedimentary, hypabyssal, and volcanic rocks above the Kukri erosion surface is therefore 3080–3870 m.

[8] In the Shackleton Glacier region, post-Mesozoic faulting is documented where NW striking normal faults and NE striking transfer faults offset Beacon strata and Ferrar sills [Barrett, 1965; La Prade, 1969; Miller et al., 2001]. The NW striking North Boundary fault places Beacon strata in contact with basement granitoids; correlative Beacon units in the Prince Olav Mountains lie 29 km south and ~2.5 km higher in elevation. Previous workers

hypothesized that the North Boundary fault is the range's master fault and has accommodated 3.1–5.2 km of total throw since the Permian assuming footwall Beacon strata dip uniformly 3°–5° south [Barrett, 1965; La Prade, 1969]. However, it is likely that fault(s) with significant throw exist north of Cape Surprise of which the so-called North Boundary fault is possibly just a subsidiary fault [McGregor, 1965]. Kinematic analysis on faults near Cape Surprise indicate NNE extension (020°–040°) [Miller et al., 2001]. Inboard (south) of the TAM front and the Prince Olav Mountains, four widely spaced range-parallel faults, including the Mount Rosenwald fault, have been mapped (Figure 1) [La Prade, 1969]. These faults strike NNW to NW and have <150 m throw each. Suspected faults between Roberts Massif and the northern side of Bennett Platform, also contribute up to 800 m of down-to-the-north displacement of middle to late Cenozoic(?) Sirius Group glacial sediments [Hambrey et al., 2003]. A large fault is inferred to lie along the Shackleton Glacier [Fitzgerald and Baldwin, 1997], vertically displacing the Kukri erosion surface <500 m [see La Prade, 1969] and separating basement with contrasting Sm–Nd model ages [Borg et al., 1990].

4. Thermochronologic Analysis and Interpretation

[9] AFT thermochronology is a well-established method commonly applied to constrain thermal and exhumation histories of upper crustal rocks, notably in studies of tectonic and landscape evolution [e.g., Gallagher et al., 1998]. Fifty-four granitoid samples for AFT analysis were collected from the Queen Maud Batholith along a 42 km long transect between the Ross Ice Shelf coast at Cape Surprise and the Prince Olav Mountains at Mount Wade (Figure 3). Five near-vertical profiles were collected from Mount Munson at the margin of the Prince Olav Mountains, from Olds Peak in the middle of the transect, and near the coast from Pyramid Peak (informal name for unnamed peak at 84°34'12"S, 174°58'48"W), spot height 700 (84°32'52"S, 174°47'0"W) and spot height 950 (84°33'9"S, 174°15'2"W). Samples within vertical profiles were collected at 50–100 m elevation intervals and, where feasible, parallel to any known or suspected faults. Elevations were measured with a calibrated pressure altimeter accurate to ±10 m. To constrain the actual locations and displacements of faults within the TAM front, vertical profiles and other samples were collected across the structural trend of the range [Fitzgerald, 1992; Foster and Gleadlow, 1996]. Thermochronology data are presented and interpreted for each sampling profile, starting at Mount Munson and moving coastward (Table 1).

4.1. Mount Munson

[10] This profile has the greatest relief (1435 m) of the five near-vertical sections (Figure 4). The uppermost sample was collected immediately beneath the Kukri erosion surface and the lower part of the profile (<2000 m elevation)

Table 1. Apatite Fission Track Thermochronologic Sample Information and Results for Transect Between Cape Surprise and Mount Wade, Shackleton Glacier Area, Central Transantarctic Mountains^a

Sample	Elevation (m)	Number of Grains	Track Density ($\times 10^6 \text{ cm}^{-2}$)			[U] (ppm)	P(χ^2) (%)	Central Age $\pm 1\sigma$ (Ma)	Relative Error (%)	Confined Track Lengths (μm)		D _{par} (μm)	
			Standard	Fossil	Induced					Mean $\pm 1\sigma$	σ	Mean	σ
<i>Cape Surprise Vicinity</i>													
SG-6	370	25	1.590 [5338]	0.745 [991]	4.014 [5341]	32	<1	53 \pm 3	18	13.8 \pm 0.3 [105]	2.7 [21]	1.99	0.23
SG-18	595	20	1.668 [5338]	1.811 [1700]	9.342 [8767]	70	3.5	58 \pm 2	10	13.1 \pm 0.3 [120]	2.9 [24]	2.07	0.29
SG-19	340	25	1.679 [5338]	0.515 [715]	3.316 [4606]	25	14	47 \pm 2	5	12.0 \pm 0.3 [120]	3.6 [21]	1.93	0.23
SG-20	230	25	1.689 [5338]	0.470 [720]	3.351 [5132]	25	0.3	43 \pm 3	18	13.4 \pm 0.2 [144]	2.5 [27]	1.69	0.26
SG-21	405	25	1.700 [5338]	0.378 [575]	3.383 [5146]	25	21	35 \pm 2	9	13.4 \pm 0.2 [102]	2.4 [28]	1.59	0.16
<i>Spot Height 950 Vertical Profile</i>													
SG-50	950	25	1.561 [5061]	0.5224 [773]	2.828 [4184]	23	0.1	53 \pm 3	20	13.3 \pm 0.2 [102]	2.4 [21]	2.00	0.23
SG-51	855	25	1.567 [5061]	0.2536 [372]	1.698 [2490]	14	66	42 \pm 2	1	13.8 \pm 0.2 [100]	2.0 [32]	1.81	0.17
SG-52	730	5	1.574 [5061]	0.6073 [54]	4.814 [428]	38	79	36 \pm 5	0	14.5 \pm 0.3 [5]	1.2		
SG-53	630	25	1.577 [5061]	0.4843 [594]	3.952 [4847]	31	16	35 \pm 2	10	14.3 \pm 0.1 [125]	1.5 [20]	1.68	0.18
SG-54	495	25	1.583 [5061]	0.420 [519]	3.896 [4814]	31	99	31 \pm 2	0	14.4 \pm 0.1 [129]	1.3 [23]	1.72	0.19
SG-55	400	25	1.589 [5061]	0.5803 [757]	5.595 [7299]	44	99	30 \pm 1	0	14.5 \pm 0.1 [170]	1.2 [21]	1.85	0.23
<i>Spot Height 700 Vertical Profile</i>													
SG-8	700	25	1.601 [5338]	0.8585 [1101]	5.27 [6759]	37	49	47 \pm 2	2	13.1 \pm 0.3 [110]	3.3 [25]	2.03	0.15
SG-10	605	25	1.616 [5338]	0.7032 [826]	4.850 [5697]	38	9	42 \pm 2	10	13.1 \pm 0.2 [120]	2.4		
SG-11	495	25	1.627 [5338]	0.5593 [735]	3.621 [4759]	28	<0.1	45 \pm 3	21	12.6 \pm 0.3 [110]	2.8 [33]	1.91	0.23
SG-12	355	25	1.637 [5338]	0.5224 [712]	3.491 [4740]	24	77	45 \pm 2	0.3	13.9 \pm 0.2 [111]	2.1 [32]	1.59	0.17
SG-13	265	25	1.653 [5338]	0.6721 [711]	4.919 [5204]	37	<0.1	40 \pm 3	23	13.6 \pm 0.2 [110]	2.5 [25]	1.88	0.35
SG-14	185	25	1.658 [5338]	0.4302 [593]	3.205 [4418]	24	43	40 \pm 3	6	13.7 \pm 0.2 [125]	2.0 [28]	2.01	0.13
SG-2	140	25	1.58 [5338]	0.4379 [673]	2.870 [4410]	20	12	44 \pm 2	4	13.8 \pm 0.3 [105]	2.7 [21]	1.94	0.23
<i>Between Spot Height 700 and Pyramid Peak</i>													
SG-9	655	25	1.611 [5338]	0.1423 [208]	1.094 [1599]	9	14	39 \pm 3	21	13.4 \pm 0.2 [36]	1.7 [21]	1.73	0.23
SG-48	370	25	1.555 [5061]	0.6504 [954]	4.942 [7248]	40	6	37 \pm 2	10	13.8 \pm 0.2 [111]	2.1 [25]	1.78	0.20
SG-44	370	25	1.542 [5061]	0.7669 [1095]	5.983 [8543]	49	20	36 \pm 1	8	13.3 \pm 0.2 [100]	2.2 [25]	1.91	0.30
SG-47	470	25	1.548 [5061]	0.7798 [1164]	6.407 [9564]	52	52	34 \pm 1	2	13.5 \pm 0.2 [106]	2.2 [25]	1.93	0.25
<i>Pyramid Peak Vertical Profile</i>													
SG-37	780	25	1.681 [5344]	1.033 [1522]	8.729 [12860]	65	75	36 \pm 1	0.9	13.6 \pm 0.1 [130]	1.5 [23]	2.01	0.24
SG-38	660	25	1.691 [5344]	1.297 [1647]	10.05 [12762]	74	<0.1	41 \pm 2	13	13.7 \pm 0.2 [137]	1.9 [25]	1.94	0.30
SG-39	565	25	1.701 [5344]	0.7233 [1089]	6.184 [9311]	45	75	36 \pm 1	0.1	14.4 \pm 0.2 [105]	1.6 [28]	2.07	0.21
SG-40	460	25	1.517 [5061]	0.3951 [538]	3.051 [4154]	25	63	36 \pm 2	2	14.4 \pm 0.1 [100]	1.2 [28]	1.70	0.16
SG-41	365	25	1.523 [5061]	0.360 [486]	3.350 [4522]	28	4.9	30 \pm 2	15	14.6 \pm 0.1 [102]	1.1 [32]	1.64	0.17
SG-42	300	25	1.530 [5061]	0.3463 [481]	3.297 [4579]	27	97	29 \pm 2	0.1	14.2 \pm 0.1 [100]	1.1 [21]	2.07	0.23

Table 1. (continued)

Sample	Elevation (m)	Number of Grains	Track Density ($\times 10^6 \text{ cm}^{-2}$)			[U] (ppm)	P(χ^2) (%)	Central Age $\pm 1\sigma$ (Ma)	Relative Error (%)	Confined Track Lengths (μm)		D _{par} (μm)	
			Standard	Fossil	Induced					Mean $\pm 1\sigma$	σ	Mean	σ
SG-43	255	25	1.536 [5061]	0.3756 [506]	3.626 [4886]	30	78	29 \pm 1	0.4	14.3 \pm 0.1 [106]	1.0		
<i>Between Pyramid Peak and Olds Peak</i>													
SG-70	335	25	1.596 [5061]	0.7256 [972]	6.788 [9093]	53	53	31 \pm 1	1.5	14.1 \pm 0.2 [145]	1.9	2.00 [28]	0.21
<i>Olds Peak Vertical Profile</i>													
SG-23	1480	25	1.586 [5344]	0.643 [883]	4.585 [6297]	36	1	41 \pm 2	16	14.3 \pm 0.1 [110]	1.5	2.26 [20]	0.18
SG-25	1385	25	1.596 [5344]	0.5104 [795]	3.589 [5591]	28	11	41 \pm 2	9	14.0 \pm 0.1 [110]	1.3	2.09 [23]	0.19
SG-26	1315	25	1.601 [5344]	0.2927 [462]	2.183 [3445]	17	92	39 \pm 2	<0.1	13.7 \pm 0.2 [80]	2.0		
SG-27	1240	25	1.616 [5344]	0.7929 [1091]	6.037 [8306]	47	88	39 \pm 1	<0.1	13.8 \pm 0.2 [130]	1.9		
SG-28	1115	25	1.621 [5344]	0.7678 [875]	6.106 [6959]	47	1	37 \pm 2	14	13.6 \pm 0.2 [100]	1.6	1.91 [25]	0.25
SG-29	1000	14	1.631 [5344]	1.144 [490]	8.715 [3733]	67	3	39 \pm 3	17	13.6 \pm 0.1 [105]	1.7		
SG-30	900	25	1.641 [5344]	0.8845 [1372]	6.954 [10787]	53	52	38 \pm 1	0.1	13.5 \pm 0.1 [140]	1.7	2.19 [23]	0.24
SG-31	800	25	1.651 [5344]	0.9977 [1286]	7.726 [9958]	59	96	39 \pm 1	<0.1	13.8 \pm 0.1 [115]	1.4	2.58 [25]	0.25
SG-32	695	25	1.666 [5344]	1.477 [1998]	12.12 [16389]	91	0.1	37 \pm 1	12	13.4 \pm 0.1 [151]	1.7		
SG-33	575	25	1.676 [5344]	1.520 [1859]	12.98 [15871]	97	19	36 \pm 1	4	13.6 \pm 0.2 [130]	1.8	1.95 [25]	0.35
<i>Mount Munson Vertical Profile</i>													
SG-127	2615	15	1.410 [5065]	3.688 [3447]	12.17 [11376]	108	10	77 \pm 2	0.5	12.4 \pm 0.2 [211]	2.7	2.36 [22]	0.28
SG-128	2495	20	1.432 [5065]	1.895 [2152]	8.739 [9925]	76	0.9	55 \pm 2	10	12.0 \pm 0.3 [160]	3.3	2.14 [30]	
SG-129	2395	20	1.453 [5065]	3.094 [3574]	13.04 [15059]	112	26	62 \pm 2	3	12.0 \pm 0.2 [150]	2.6	2.28 [28]	0.32
SG-130	2285	20	1.486 [5065]	1.779 [1706]	9.504 [9116]	80	92	50 \pm 2	<1	12.6 \pm 0.2 [130]	2.7	2.25 [30]	
SG-131	2180	25	1.496 [5065]	1.779 [2595]	10.23 [14928]	86	0	48 \pm 2	13	12.6 \pm 0.2 [150]	2.7	2.33 [23]	0.19
SG-132	2055	20	1.518 [5065]	1.977 [1848]	14.63 [13673]	121	50	37 \pm 1	<0.1	12.9 \pm 0.3 [120]	3.0		
SG-133	1955	25	1.539 [5065]	0.859 [1173]	8.115 [11081]	66	97	30 \pm 1	0	14.6 \pm 0.2 [105]	1.5	2.19 [144]	0.24
SG-134	1860	25	1.561 [5065]	0.5603 [664]	6.053 [7173]	49	99	26 \pm 1	0	14.0 \pm 0.2 [139]	1.1	1.96 [22]	0.28
SG-135	1765	25	1.591 [5065]	0.7719 [1012]	7.523 [9863]	59	94	30 \pm 1	<0.1	14.4 \pm 0.1 [110]	1.3		
SG-136	1595	25	1.604 [5065]	0.7458 [985]	7.578 [10008]	59	100	29 \pm 1	0	14.3 \pm 0.1 [115]	1.1		
SG-137	1490	25	1.626 [5065]	1.312 [1460]	9.098 [10120]	70	3	43 \pm 2	11	12.6 \pm 0.2 [110]	2.2	1.62 [23]	0.24
SG-138	1340	25	1.658 [5065]	0.737 [818]	5.511 [6116]	42	0	41 \pm 3	23	12.0 \pm 0.2 [110]	2.1		
SG-139	1130	25	1.669 [5065]	1.103 [918]	8.347 [6945]	63	7	40 \pm 2	11	13.0 \pm 0.2 [115]	2.6	2.07 [32]	0.17
<i>Mount Wade</i>													
SG-140	2000	25	1.690 [5065]	0.5629 [719]	2.992 [3822]	22	99	58 \pm 3	0.01	12.8 \pm 0.3 [115]	2.8	2.05 [23]	0.19

crosses a number of small cols where crush zones of granite and slickensided surfaces were observed. AFT ages range from 77 ± 2 Ma (age errors quoted at 1σ throughout the text) for the uppermost sample to 26 ± 1 Ma (Table 1). Above 2000 m elevation, the confined track length distributions (CTLD) are left-skewed, indicating the presence of short tracks (Figure 4). Overall, short mean lengths ($12.0 - 12.9 \mu\text{m}$), large σ ($>2.6 \mu\text{m}$), and a gentle slope on the age-elevation plot (16 ± 2 m/Myr; error quoted at 2σ level) indicate considerable residence time in the apatite PAZ. Between elevations of 2000 and 1500 m, the steeper age-elevation relation and the CTLDs' longer means ($>14.0 \mu\text{m}$), smaller σ ($<1.5 \mu\text{m}$), and weaker skewness indicate relatively rapid cooling. The upper part of the profile represents a classic exhumed PAZ [Fitzgerald and Gleadow, 1990] with the break in slope marking the onset of “rapid” cooling between 37 and 30 Ma. It is difficult to more tightly constrain the onset of more rapid cooling because SG-132 (37 ± 1 Ma) lies within, but near the base of, the exhumed PAZ as indicated by the presence of shorter tracks whereas SG-133 (30 ± 1 Ma) lies below the base of an exhumed PAZ.

[11] The lowest three samples of the Munson profile have ages and CTLDs similar to those within the exhumed PAZ. Combined with observations of crush zones, altered granite, and slickensides, we infer the age-elevation pattern is disrupted by at least three faults with individual throws of ~ 700 m, ~ 120 m, and ~ 200 m down toward the coast. Closer to the summit, between SG-128 and SG-129, there is also a possible fault with 100–200 m throw, also down toward the coast.

[12] For rapidly cooled samples below the break in slope, a least squares regression through the age-elevation data indicates an apparent denudation rate of ~ 50 m/Myr. Apparent denudation rates derived from age-elevation plots can overestimate the true denudation rate due to advection and topographic effects [e.g., Stüwe et al., 1994; Mancktelow and Grasemann, 1997; Braun, 2002; Reiners et al., 2003]. However, for a topographic wavelength of ~ 8 km, an average along-strike value for the TAM front east of the Shackleton Glacier (Figure 1), the topographic-advection correction is small ($\sim 5\%$) and therefore ignored [Reiners et al., 2003].

[13] Temperature-time paths for individual samples were inverse modeled using AFTSolve [Ketcham et al., 2000]

using the annealing algorithm of Ketcham et al. [1999] for comparison with our interpretations of age-elevation plots and to better constrain the onset of rapid cooling. Therefore, only samples older than the age of the break in slope were modeled. D_{par} , which is the maximum etch pit diameter parallel to the c axis, age, and length data served as input data (see Figure 5). The best fit modeled cooling envelope indicates cooling rate increased from 0.7 to $0.8^\circ\text{C}/\text{Myr}$ to $6 - 10^\circ\text{C}/\text{Myr}$ at $30 - 35$ Ma (Figure 5). This change is more obvious in samples close to the age of the break in slope because these contain a greater proportion of rapidly cooled tracks. Interestingly, although the change in cooling rate is obvious in an age-elevation plot, it is not obvious in the T - t models for the higher elevation samples, lying a mere 300 m or so above the break in slope, indicating one danger in relying on models from single samples to constrain thermal histories.

4.2. Olds Peak

[14] Samples from Olds Peak were collected nearly parallel to the strike of the TAM front over an elevation range of 905 m. AFT ages ranges from 41 ± 2 Ma at the summit to 36 ± 1 Ma at glacier level (Figure 4). Both the steep slope (~ 200 m/Myr) on an age-elevation plot of these samples and weakly skewed CTLDs with long means ($>13.4 \mu\text{m}$) and small σ ($<2.0 \mu\text{m}$) suggest relatively rapid cooling. Mean track lengths of the uppermost samples are $>14.0 \mu\text{m}$ and there is no obvious break in slope in the profile, indicating rapid cooling began before $\sim 41 \pm 2$ Ma. Mean track lengths decrease with decreasing elevation suggesting that cooling may have slowed slightly by 36 Ma.

4.3. Pyramid Peak

[15] Samples on Pyramid Peak were collected down a steep ridge oriented oblique to local faults. All samples have apparent ages <41 Ma (Figure 6), with the youngest age of 29 ± 1 Ma coming from the lowest sample. Only the top two samples, with mean lengths $<13.7 \mu\text{m}$ and $\sigma > 1.5 \mu\text{m}$, show evidence for partial annealing. Lower elevation samples have weakly skewed CTLDs with longer means ($>14.2 \mu\text{m}$) and smaller σ ($<1.6 \mu\text{m}$) indicative of rapid cooling. For this profile, we therefore conclude rapid cooling began between 41 and 36 Ma. No field evidence for faults was observed. However, a slight kink at the base

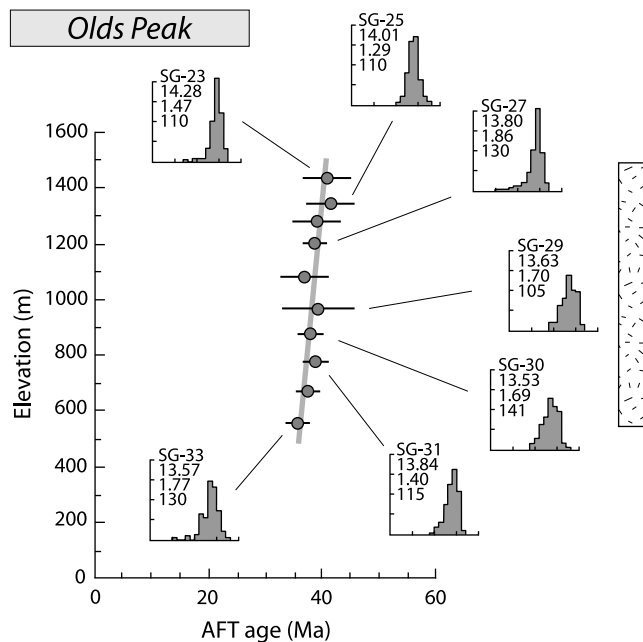
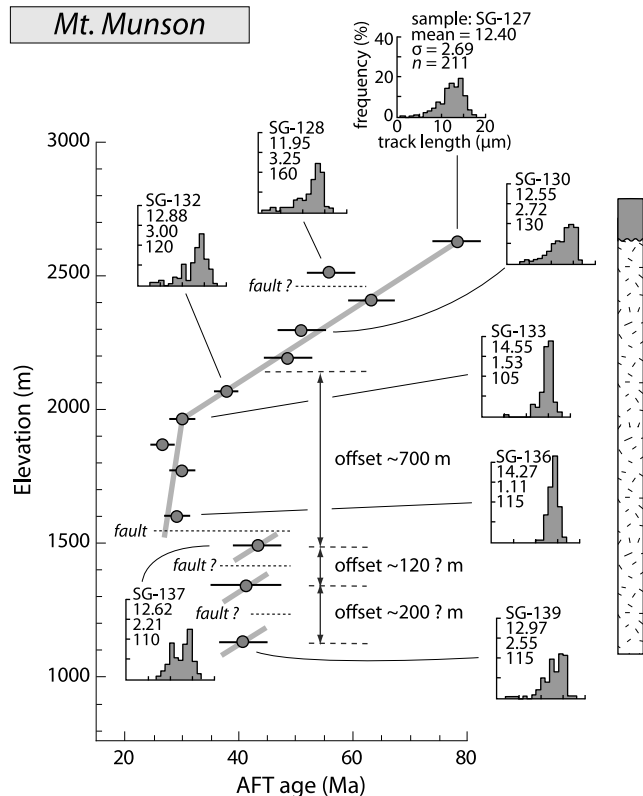
Notes to Table 1:

^aApatite grains were separated from their host rocks using conventional magnetic and heavy liquid techniques. Grains were mounted in epoxy on glass slides, polished to expose internal surfaces, and etched in 5 M HNO_3 to reveal fossil fission tracks. Prepared samples were irradiated in the Oregon State University TRIGA reactor, in which neutron fluences were monitored using the Corning CN-5 uranium glass standard. Standard, fossil, and induced track densities were measured for individual grains using the external detector method [e.g., Gleadow, 1981] with a Nikon Optiphot-2 transmitted and reflected light petrographic microscope at $1250 \times$ magnification under a dry $100 \times$ objective, outfitted with a computer-controlled Kinetek stage operating with FT Stage software by Dumitru [1993], a drawing tube, and digitizing tablet. Ages were calculated using the zeta calibration method [Hurford and Green, 1983]. Central ages are reported [Galbraith and Laslett, 1993]; analytical error reported at the 1σ level; σ , standard deviation; values in brackets are n , number of tracks counted or measured. Relative error is a measure of the age dispersion of the single-grain ages combined within the sample age; low relative errors ($<10\%$) of the central age indicate individual grain ages are drawn from a single age population [Galbraith and Laslett, 1993]. The chi-square (χ^2) test was used judge whether the ages of individual grains were drawn from a population with a Poisson distribution. For values of $P(\chi^2) \geq 5\%$, the test fails to reject the hypothesis that the data do not differ significantly from a Poisson distribution. Horizontal, confined track length measurements were made following the method outlined by Laslett et al. [1982] and Laslett et al. [1984]. D_{par} is the diameter of fission track etch figures parallel to the c axis [Burtner et al., 1994; Carlson et al., 1999; Ketcham et al., 1999].

of the age-elevation plot could be the result of minor down-to-the-south faulting or an increase in denudation rate at ~ 30 Ma.

4.4. Spot Height 700

[16] Samples on spot height 700 were collected down a profile oriented slightly oblique to local faults. These



samples yield apparent ages ≥ 40 Ma and all CTLDs are left-skewed with numerous short tracks (mean $< 13.9 \mu\text{m}$ and $\sigma > 2.0 \mu\text{m}$), indicating they likely reside in an exhumed PAZ (Figure 6). The relatively steep slope of the age-elevation plot may be the result of down-to-the-northwest or down-to-the-northeast faulting within the profile. A similar inferred fault lies in a gully just south of the summit (Figure 7) and separates two samples at similar elevations: a 39 Ma sample (SG-9) to the south from a 47 Ma sample (SG-8) to the north, consistent with down-to-the-northeast faulting.

4.5. Spot Height 950

[17] Samples on spot height 950 were collected on a steep topographic slope parallel to the strike of significant local faults. The age-elevation profile, combined with CTLDs, shows a break in slope and a transition from partially annealed to rapidly cooled samples between 42 ± 2 Ma and 36 ± 1 Ma (Figure 6). Above the break in slope, CTLDs are left-skewed with short means ($< 13.8 \mu\text{m}$) and large σ ($> 2.0 \mu\text{m}$). Below the break in slope, longer mean track lengths ($> 14.3 \mu\text{m}$), smaller σ ($< 1.5 \mu\text{m}$), and minimal skewness are consistent with faster cooling. A least squares regression of sample elevation versus age below the break in slope yields an apparent denudation rate of ~ 70 m/Myr.

[18] Collectively, the three profiles closest to the coast indicate that rapid cooling began there at ~ 40 Ma. In the middle of the TAM front, samples at Olds Peak were cooling rapidly at ~ 40 Ma but there is no indication of exactly when the onset of rapid cooling was or if it is distinguishable from the coastal profiles. In contrast, the onset of rapid cooling at Mount Munson on the inland side of the TAM front was between 35 and 30 Ma.

5. Occurrences and Characteristics of Piedmont Erosion Surfaces

[19] The modern geomorphology of the TAM reflects landscape evolution that postdates the AFT record. Between the Prince Olav Mountains and Ross Ice Shelf, piedmont summits and ridges rise steeply from adjacent valley glaciers. In contrast with this steep topography are erosion or planation surfaces [e.g., *Burbank and Anderson, 2001*] that cap many piedmont ridges and summits (Figure 8a) or form broad, flat valley floors slightly lower than adjacent summits (Figure 8b). For purposes of this study, we defined erosion surfaces to be characterized by (1) low relief and gentle slopes that stand in sharp contrast with surrounding,

Figure 4. Sample elevation versus AFT age plots for vertical profiles on Mount Munson and Olds Peak with selected confined track length distribution (CTLD) histograms. Errors on AFT ages given at 2σ level. Thick gray lines mark general trends. CTLD statistics and scales labeled for summit sample on Mount Munson: σ , confined track length standard deviation; n , number of track lengths measured. Tectonostratigraphic columns for each profile shown at right. See Figure 7 for key to lithologic symbols.

steeper topography and (2) truncated sedimentary strata or igneous intrusions. Nineteen erosion surfaces were mapped in the field and with vertical and oblique aerial photographs (Figure 9). In general, these erosion surfaces are <600 m above modern glacier levels. Example topographic profiles of these surfaces are shown in Figure 10. Individually, relict erosion surfaces in the piedmont have slopes that range from <1° to 15°, in sharp contrast with much steeper subjacent slopes, which are >20° (Figure 10). These erosion surfaces occur on all lithologies in the TAM front. At Cape Surprise, erosion surfaces truncate Beacon beds and Ferrar Dolerite sills and have a thin or absent mantle of frost-shattered regolith. Elsewhere, regolith or till is thicker and contains ice wedge polygons (Figure 8a). The surfaces are

generally <0.5 km² in area, but several range from 5 to 10 km². In total, recognized piedmont erosion surfaces between the Shackleton and Liv glaciers cover an area of 46.7 km².

[20] Viewed together, these piedmont erosion surfaces have nearly accordant elevations and extend discontinuously from the base of the Prince Olav Mountains to the Ross Ice Shelf (Figure 11). Mean elevations of individual surfaces are shown in Figure 9 and range from 1410 m at the base of the Prince Olav Mountains to 430–750 m along the ice shelf. As a whole, these define an interpolated surface that slopes ~3° toward the Ross Ice Shelf (Figure 11).

6. Discussion

6.1. Thermochronologic Constraints on Faulting Across the Transantarctic Mountains Front

[21] Paleozoic Beacon strata offset vertically between Cape Surprise and the Prince Olav Mountains only very broadly constrain potential fault locations and the history of fault movement in the mostly granitic TAM front. More detail of TAM front structure can be achieved with AFT isochrones superimposed onto a cross section, where isochrones offset vertically over short horizontal distances indicate fault throw or block tilting [e.g., *Fitzgerald*, 1992; *Foster and Gleadow*, 1996]. To constrain vertical offset with some confidence, we used only isochrones from the exhumed PAZ, where there is significant age variation with elevation [e.g., *Fitzgerald*, 1992]. To do this, we identified the 40 and 50 Ma AFT isochrones between the Prince Olav Mountains and Cape Surprise (Figure 12b). The 40 Ma isochrone, near the base of the exhumed PAZ, provides the greatest detail across the entire TAM front because older AFT ages are uncommon near the coast and absent in the central portion of the TAM front (Figure 12a). Significant discontinuities in the isochrones coinciding with valleys or other topographic discontinuities were interpreted as faults. The interpreted composite cross section in Figure 12b shows that the TAM front at this longitude,

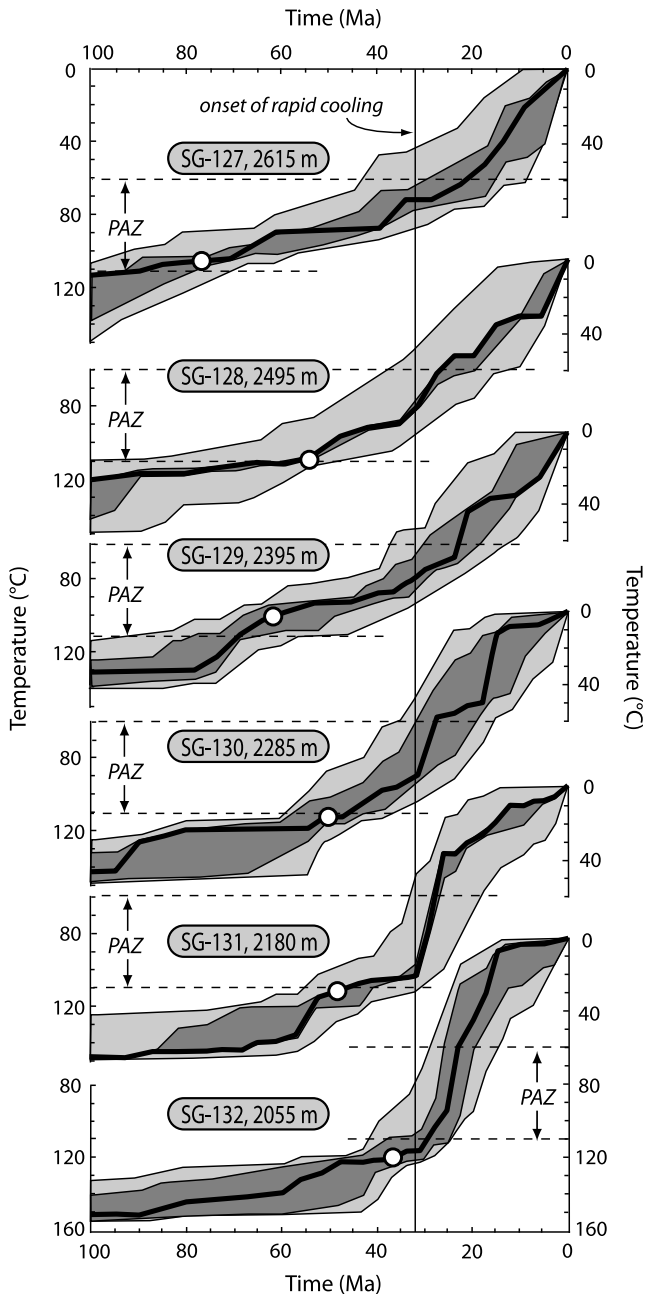


Figure 5. Inverse model T - t histories for AFT samples on Mount Munson, arranged according to sample elevation. Thick line is the best fit; dark gray region is a good fit (i.e., supported by the data); light gray region is an acceptable fit (i.e., not ruled out by the data). Thin dashed horizontal lines represent paleo-PAZ; vertical line marks approximate onset of rapid cooling. White circles on T - t paths mark each sample's central ages. Models were run with a starting track length of 15.5 μm . For the Mount Munson profile, D_{par} varies from 1.62 to 2.36 μm with a mean of 2.13 μm . For comparison, D_{par} for the Durango apatite and Fish Canyon Tuff age standards measured using these same etching conditions was 2.02 and 2.35 μm , respectively. This compares to 1.83 and 2.43 μm measured by *Donelick et al.* [1999] using the etching conditions for which AFTSolve is calibrated. The similarity of measurements, with one slightly longer and one slightly shorter, meant that we did not adjust our D_{par} values for model input. No preset cooling intervals were defined.

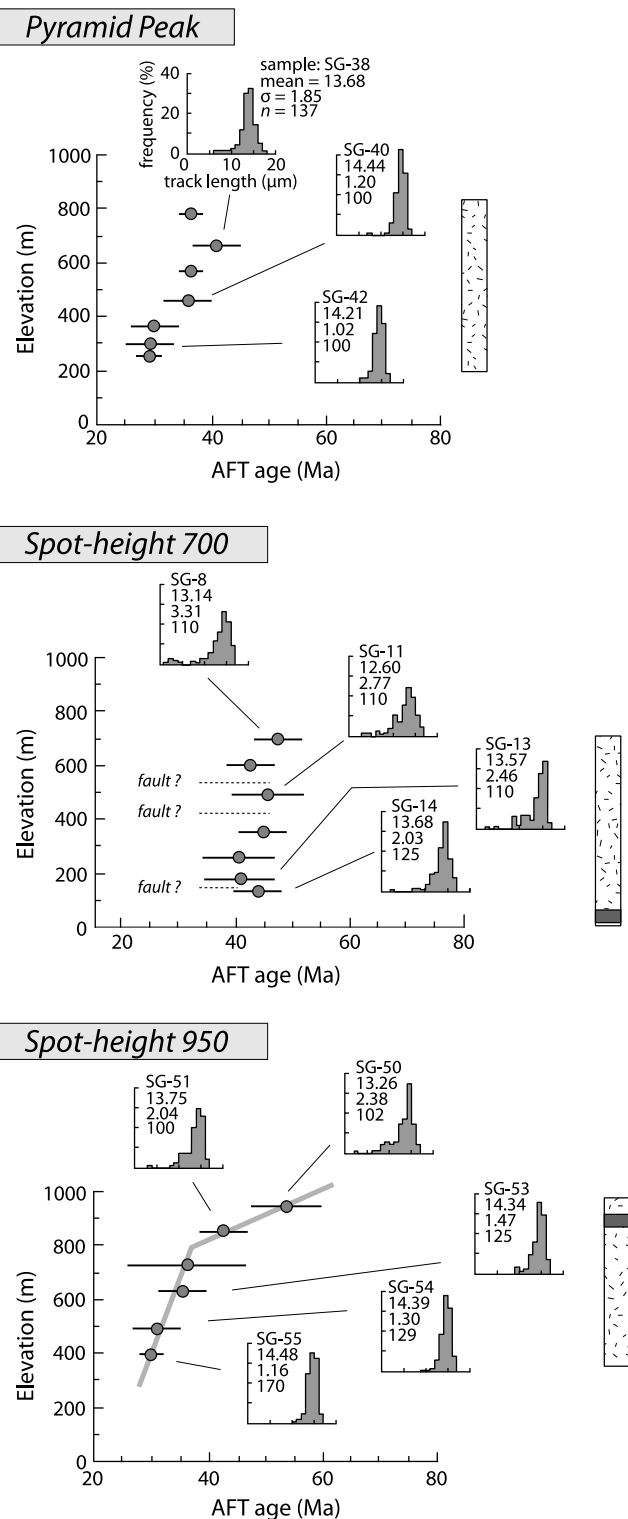


Figure 6. Graphs of sample elevation versus AFT age for vertical profiles on Pyramid Peak, spot height 700, and spot height 950. See Figure 4 caption for further details.

inboard of Cape Surprise, consists of at least nine significant normal faults spaced 1–10 km apart over a fault zone 20–30 km wide. This result contrasts with earlier interpretations of the TAM front at this location that assumed all throw was across a single master fault [McGregor, 1965; La Prade, 1969]. However, the step-faulted structure of the TAM front in the Shackleton Glacier area is similar to the in the Scott Glacier region, Beardmore Glacier region, and southern Victoria Land (Figure 1b) [Gunn and Warren, 1962; Barrett, 1965; Katz, 1982; Gleadow and Fitzgerald, 1987; Fitzgerald, 1992, 1994; Fitzgerald and Stump, 1997].

[22] The offset isochrones show a large amount of fault displacement is Cenozoic but alone they do not constrain any earlier history of faulting. To estimate the amount of pre-Cenozoic faulting, we compare total stratigraphic and isochrone displacements across the TAM front. The 55 Ma isochrone spans the greatest distance across the range front, being present at both Mount Munson and just south of Cape Surprise (near SG-6) in the footwall of the North Boundary fault. This isochrone is vertically separated between these two locations by 2095 ± 170 m. This confidence interval of ± 170 m was determined by multiplying the age-elevation slope of exhumed PAZ (16 ± 2 m/Myr; 2σ) by the 2σ error on the AFT age and propagating errors.

[23] To constrain the total offset from Mount Munson to Cape Surprise, we have to include throw across the North Boundary fault. The North Boundary fault places the 55 Ma isochrone, which is 120 ± 70 m below the Kukri erosion surface on Mount Munson, in contact with the Fairchild Formation, which is 140–378 m above the Kukri erosion surface [Barrett, 1965; La Prade, 1969]. Throw on this normal fault is therefore 200–600 m. Adding this figure to the measured isochrone offset above, cumulative vertical offset of the 55 Ma isochrone along this cross section, corresponding approximately to C-C' in Figure 12, is 2.3–2.7 km. By comparison, cumulative stratigraphic offset between Mount Munson and Cape Surprise is 2.4–2.6 km. For these estimates, we assume that both the Kukri erosion surface and isochrones in the exhumed PAZ were approximately horizontal prior to faulting. Because offset of the 55 Ma isochrone is within error of 100% of the total stratigraphic offset, we conclude that all offset postdates 55 Ma. Because the exhumed PAZ indicates a period of relative thermal and tectonic stability, it is likely that all offset actually postdates the onset of rapid cooling at ~ 40 Ma.

[24] Evidence for Mesozoic extension has been reported along the TAM, including the Beardmore Glacier region [Wilson, 1992; Elliot and Larsen, 1993; Wilson, 1993] and southern Victoria Land [Mortimer et al., 2002], but extension at that time appears minor and generally inland of the TAM front, in the hinterland. Our AFT data indicate no significant normal faulting occurred in the TAM front between the late Paleozoic and the early Cenozoic. Therefore, Mesozoic extension in the Shackleton Glacier area was either confined to the hinterland or minor overall.

6.2. Estimates and Patterns of Denudation

[25] With a few reasonable assumptions, the paleodepth of the base of an exhumed PAZ can be calculated and an

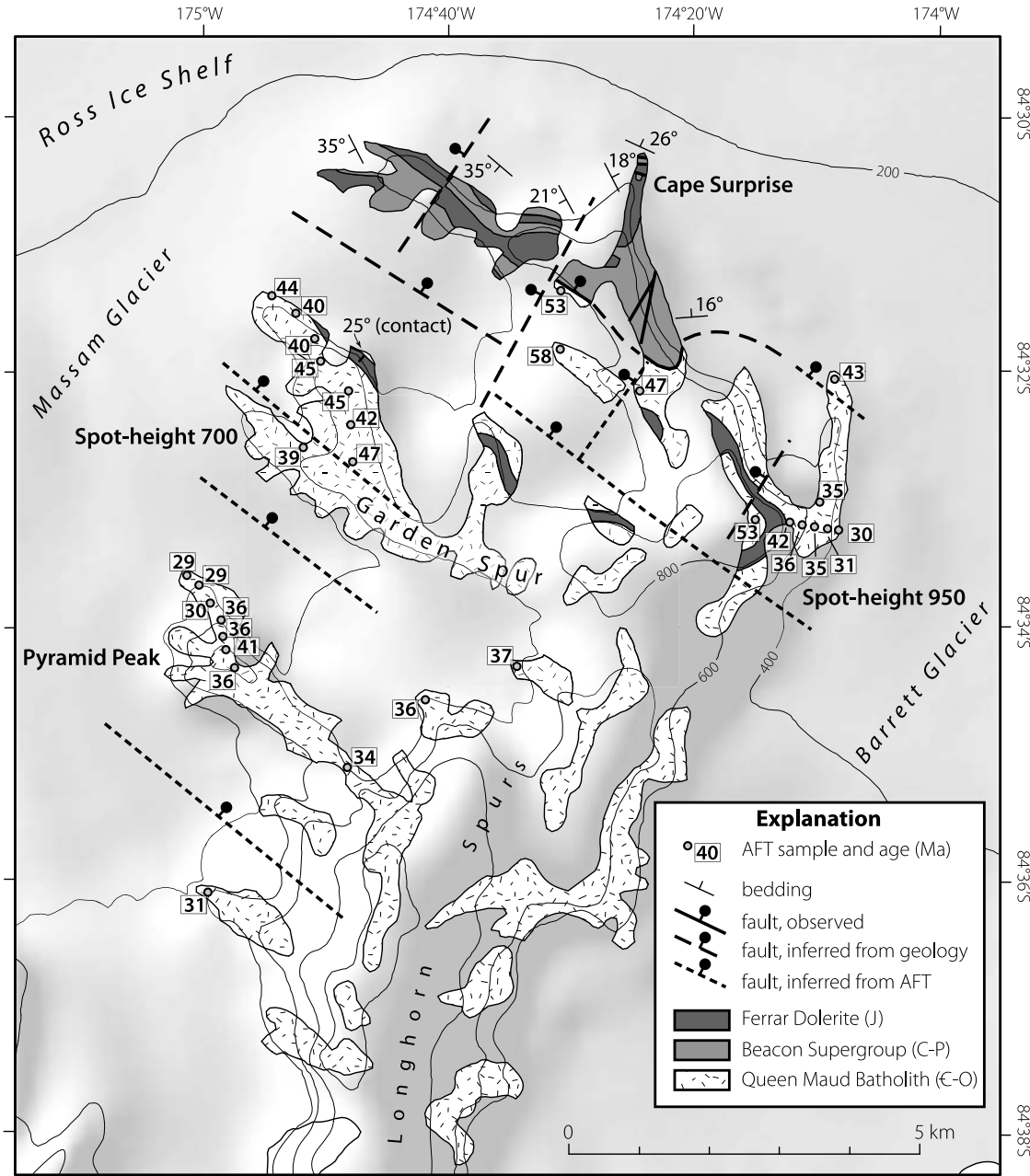


Figure 7. Geological map with shaded relief of the Cape Surprise area, showing locations of AFT samples, their central ages, and local structure. Geology is after Barrett [1965], La Prade [1969], and Miller *et al.* [2001]. Contour interval is 200 m.

estimate of the amount of denudation since the Eocene determined. Following on from earlier studies in the TAM that assume an Eocene geothermal gradient (20° – $25^{\circ}\text{C}/\text{km}$), a mean annual Eocene surface temperature (0°C), and a temperature (110°C) for the base of the apatite PAZ [e.g., Fitzgerald, 1992, 1994], the exhumed PAZ was at a depth of 4.4–5.5 km at the onset of rapid cooling (~ 40 Ma). Because the exhumed PAZ is ~ 0.5 km above the mean modern bedrock surface in the center of the study area near Olds Peak and Mount Munson (Figure 12d), a maximum of

4.9–6.0 km of total denudation has occurred there since ~ 40 Ma. Denudation profiles across the TAM comparing this thermochronologic estimate with a stratigraphic estimate are shown in Figure 12c. This estimate of Cenozoic denudation is comparable to elsewhere along the TAM, where it ranges from 4 to 9 km [e.g., Fitzgerald, 1992, 1994; Fitzgerald and Stump, 1997]. These thermochronologic results are also consistent with local geologic constraints. Considering that the base of the exhumed PAZ is 0.6–0.7 km below the Kukri erosion surface on Mount Munson,

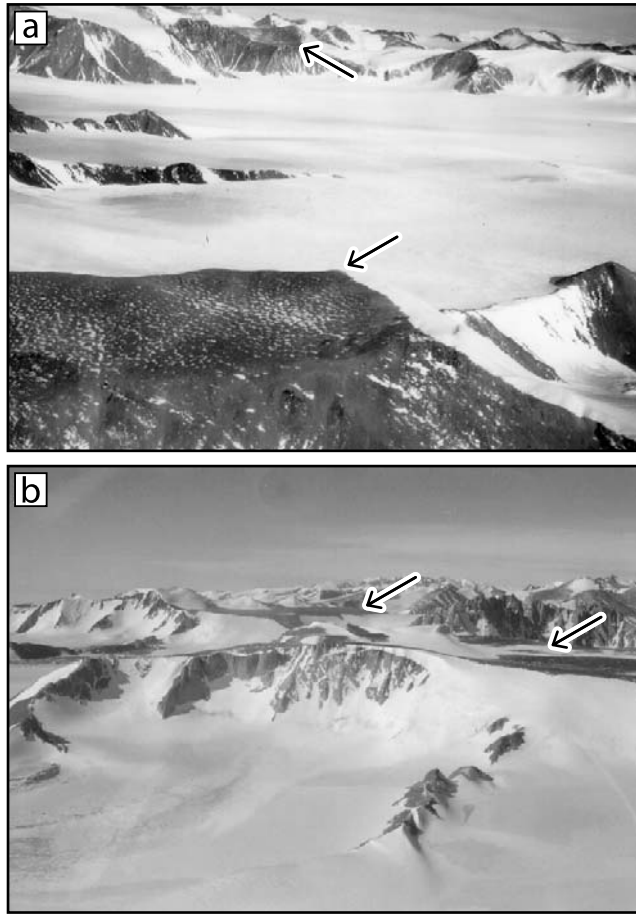


Figure 8. Photographs of piedmont erosion surfaces, marked with arrows. (a) Flat summit of spot height 720 in the Gabbro Hills (foreground) and undulating, low-relief surface of Longhorn Spurs (background). View toward west. (b) Broad flat surface of Mount Skinner (foreground) and flat valley bottom in the Lillie Range (background). View toward east.

the Kukri erosion surface would have been 3.7–4.9 km deep at the end of the Eocene based on assumed geothermal and thermochronologic parameters. This compares closely to the combined thickness of Beacon strata, Ferrar sills, and Kirkpatrick flows (3.1–3.9 km), the overburden at the end of the Jurassic assuming uniform thickness. These results suggest minimal denudation during the Cretaceous. Supporting this, $^{40}\text{Ar}/^{39}\text{Ar}$ analyses of K-feldspar from the study area also indicate no significant cooling prior to the Cenozoic [Baldwin et al., 1999]. The lack of detectable Cretaceous denudation is consistent with evidence for no significant normal faulting during this time.

[26] Interestingly, the onset of rapid cooling, determined by the age of exhumed PAZ, gets younger landward, from ~40 Ma near Cape Surprise to 30–35 Ma at Mount Munson. This younging trend may be the result of such end-member scenarios as passive escarpment retreat or an erosional front that tracked a landward migration in fault activity and consequent local relief generation. Averaged

over the 5–10 Myr span, inferred lateral migration of the cooling front occurred at a rate of 3–6 km/Myr, similar to other estimated long-term rates of escarpment retreat of 1–7 km/Myr [Cole and Mayer, 1982; Ballantyne and Kirkbride, 1987; Schmidt, 1988, 1989; Gilchrist and Summerfield, 1990; Steckler and Omar, 1994; Gallagher et al., 1995; Weissel and Seidl, 1997].

6.3. Origin of Piedmont Erosion Surfaces

[27] Erosion surfaces, broadly similar in elevation, morphology, and lithology to those documented in the study area, have also been identified in coastal southern Victoria Land [Sugden et al., 1995; Sugden and Denton, 2004], northern Victoria Land [van der Wateren et al., 1996], and near the Nimrod Glacier in the central TAM (Figure 1b) [Laird, 1963]. In the Shackleton Glacier region, but south of the Prince Olav Mountains, Hambrey et al. [2003] identified a surface between 1850 m and 2200 m elevation eroded into Ferrar Dolerite on Bennett Platform and Roberts Massif (Figure 1a), which they termed the “Shackleton erosion surface.” These surfaces and others in West Antarctica have been attributed to a variety of origins: marine abrasion [LeMasurier and Landis, 1996; van der Wateren et al., 1996; Wilson and Luyendyk, 2006], glacial erosion [Laird, 1963] or fluvial processes and slope wash [Denton et al., 1993; Sugden et al., 1995; Sugden and Denton, 2004].

[28] Within our study area, piedmont erosion surfaces are morphologically similar to pediments and cryopediments, which typically slope <1°–12° from mountain fronts and have lateral dimensions on the order of 1 or 10 km [Priesnitz, 1988; Cooke et al., 1993]. Accordant surface elevations suggest the piedmont erosion surfaces identified across the TAM front represent vestiges of a former, more continuous surface (a pediplain) that has been partially destroyed by valley incision. Erosion surfaces in southern Victoria Land are also interpreted as pediments or pediplains [Denton et al., 1993; Sugden and Denton, 2004]. Formation of pediments, cryopediments, or larger pediplains typically involves fluvial as well as slope processes including slope wash or solifluction [Priesnitz, 1988; Cooke et al., 1993], which is consistent with evidence for early Cenozoic stream erosion in Antarctica [Baroni et al., 2005; Jamieson et al., 2005]. We cannot rule out other possible origins but we do note that the inferred original piedmont erosion surface in our study area was much larger than typical marine terraces [e.g., Anderson et al., 1999] and strand flats [e.g., Benn and Evans, 1998] and is therefore not likely of marine origin. Nor is it likely the result of glacial erosion, which is not known to plane surfaces [Benn and Evans, 1998].

6.4. Age of Piedmont Erosion Surfaces

[29] Age constraints on the piedmont erosion surfaces are few, and reliable correlations with other erosion surfaces in the TAM remain a challenge. The surfaces must postdate the youngest AFT ages, so the surfaces are <26 Ma. Evidence suggests that similar erosion surfaces and Antarctic landforms, in general, are quite old and undergoing very slow erosion. For example, the Shackleton erosion surface

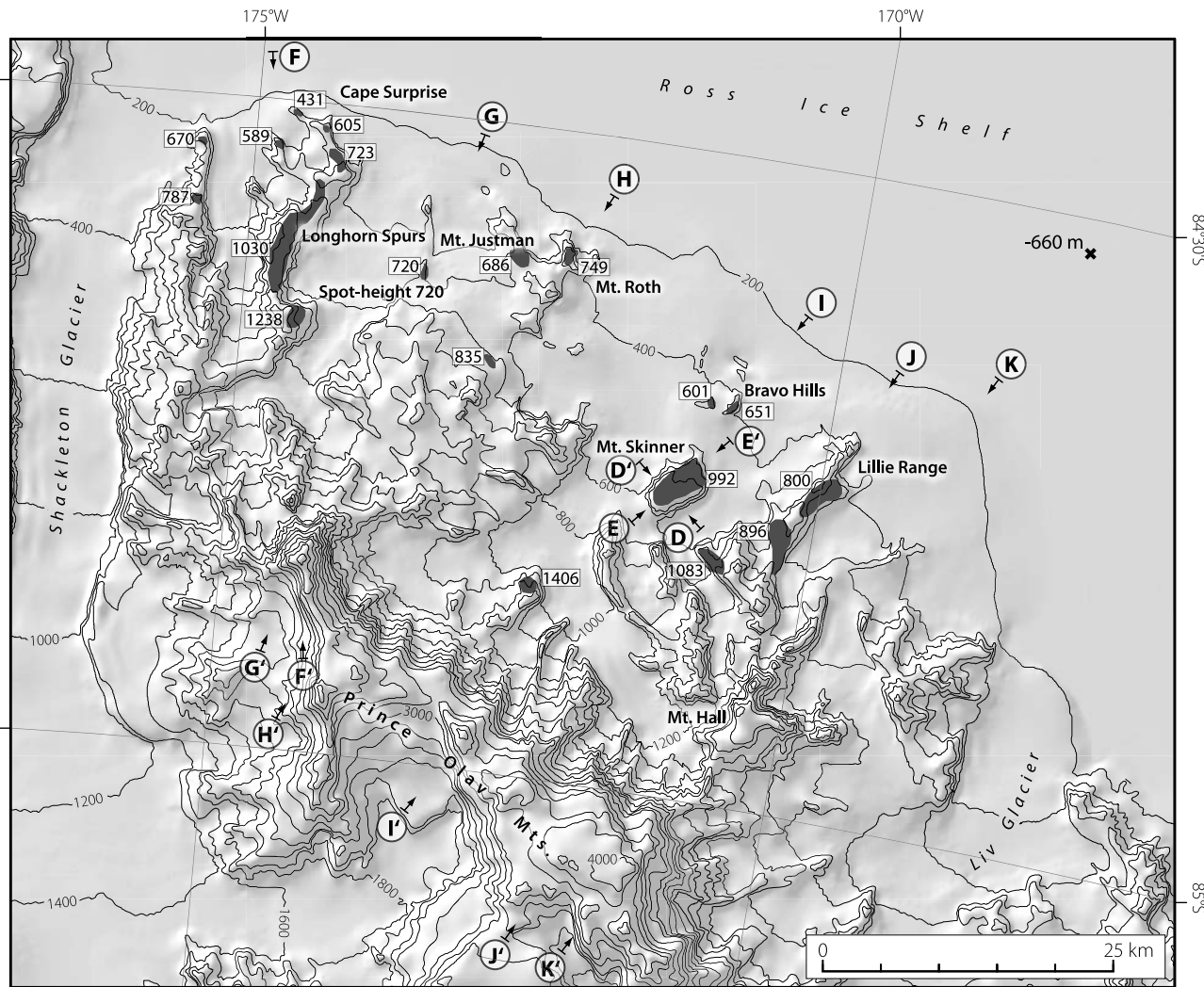


Figure 9. Map showing locations of piedmont erosion surfaces north of the Prince Olav Mountains, excluding the Kurki erosion surface. Erosion surface mean elevations (m) in boxes. Elevation of basin below Ross Ice Shelf, shown with a cross, from the Ross Ice Shelf Traverse, 1957–1958, as recorded on U.S. Geological Survey Antarctic reconnaissance series map, Shackleton Glacier SW1-10/1. Contour interval is 200 m. Locations of topographic profiles in Figures 10 and 11 are indicated.

[Hambrey *et al.*, 2003] is overlain by Sirius Group tillites with surface exposure ages >10 Ma [Kurz and Ackert, 1997]. Bedrock erosion surfaces in the Dry Valleys sector of southern Victoria Land have ^{21}Ne minimum exposure ages of 4–5 Ma and erosion rates <0.15 m/Myr [Summerfield *et al.*, 1999]. Well-dated glacial deposits in southern Victoria Land and analyses of erosion on volcanoes in Marie Byrd Land indicate little landscape modification in these regions since ~14 Ma [Marchant *et al.*, 1996; Rocchi *et al.*, 2006; Lewis *et al.*, 2007]. At ~14 Ma, the Antarctic climate became steadily frigid and therefore not conducive to much erosion except locally by warm-based glaciers. Based on these constraints, the piedmont planation surfaces in the Shackleton Glacier region are inferred to be >14 Ma but

<26 Ma. Denudation rates may have had to increase from 50 to 200 m/Myr (between ~40 and ~30 Ma) to ~250–330 m/Myr (between ~30 and ~14 Ma) to exhume the TAM front to the level of the erosion surface. These rates seem reasonable compared to elsewhere in the TAM at this time [Fitzgerald, 2002] and may leave enough time to create planation surfaces, considering that lateral planation required to produce pediments up to 50 km in length and width can occur in as few as 1–2 Ma [e.g., Hall *et al.*, 2008]. If these surfaces did form, in part, due to fluvial processes, then this suggests that fluvial erosion was active in the TAM later than previously thought (>55–34 Ma) [Jamieson and Sugden, 2008] and after the time (34 Ma) when glaciers existed locally in the TAM [Naish *et al.*,

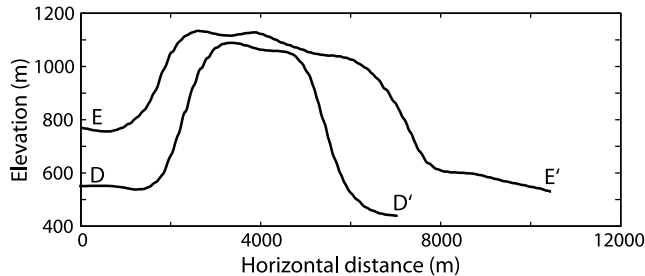


Figure 10. Topographic profiles across Mount Skinner from RAMP DEM, which has a 200 m cell size [Liu et al., 2001]. Erosion surface on E-E' slopes $\sim 3^\circ$ NE and on D-D' slopes $\sim 2^\circ$ NW, compared to side slopes of $\sim 30^\circ$. E-E' displaced 50 m higher for clarity. Vertical exaggeration is 10 \times . See Figure 9 for locations.

2001]. However, prior to maximum expansion of the East Antarctic ice sheet in the Miocene [Passchier, 2004; Sugden and Denton, 2004; Lewis et al., 2006, 2007], there is evidence of warm interglacial periods when mean summer temperatures reached $\sim 5^\circ\text{C}$ [Ashworth and Kuschel, 2003]. It is reasonable that fluvial erosion could have occurred on the piedmont during these interglacials, or even during glacial periods if glaciers were restricted to higher elevation areas such as in the Prince Olav Mountains.

6.5. Late Cenozoic Uplift and Deformation of Erosion Surfaces

[30] Formation of an erosion surface, whether fluvial or marine, requires a base level that is stable with respect to a rock reference frame to which the surfaces are graded [Burbank and Anderson, 2001]. Given the proximity of these erosion surfaces to the coast, base level was likely sea

level, and hence their present elevations are a measure of surface uplift since the time they formed minus sea level at time of formation. Although eustatic sea level estimates for much of the Cenozoic are debated [Miller et al., 2005; Spasojević et al., 2008] they provide constraints. Given that the surfaces formed between ~ 26 and ~ 14 Ma, and accounting for eustasy during this period, when sea level varied between -40 and $+140$ m relative to present-day [Kominz, 1984; Haq et al., 1987; Kominz et al., 1998; Van Sickel et al., 2004; Haq and Al-Qahtani, 2005], the 430–750 m erosion surface elevations along the ice shelf coast imply 290–790 m of surface uplift, probably on faults along the margin of the modern ice shelf. With sea level being the lowest elevation these surfaces could have formed at, this range of values is the maximum likely amount of surface uplift.

[31] The magnitude of surface uplift in the Shackleton Glacier region since ~ 14 Ma is similar to estimates of surface uplift in Victoria Land. There estimates range from <300 m since 2.6 Ma [Wilch et al., 1993] and 400–500 m since 3–5 Ma [Wrenn and Webb, 1982] to ~ 400 m since 11 Ma [Mortimer et al., 2007]. Cosmogenic nuclide data indicate that surfaces have been close to their present elevations since ~ 3 Ma in southern Victoria Land [Brook et al., 1995] and since >4 Ma in the Dominion Range of the central TAM [Ackert and Kurz, 2004]. Notably, our results contrast with estimates of 1–3 km of surface uplift in the central TAM since the Pliocene [Webb et al., 1986; Behrendt and Cooper, 1991; Webb et al., 1996; Wilson et al., 1998].

[32] The general accordance of erosion surfaces elevations between the Shackleton and Liv glaciers implies that since formation, there has been little significant deformation within the TAM front. This interpretation assumes that all erosion surfaces were graded to the same base level and are the same age. If this assumption is valid, the low elevation of the erosion surface near spot height 720 (Figure 8),

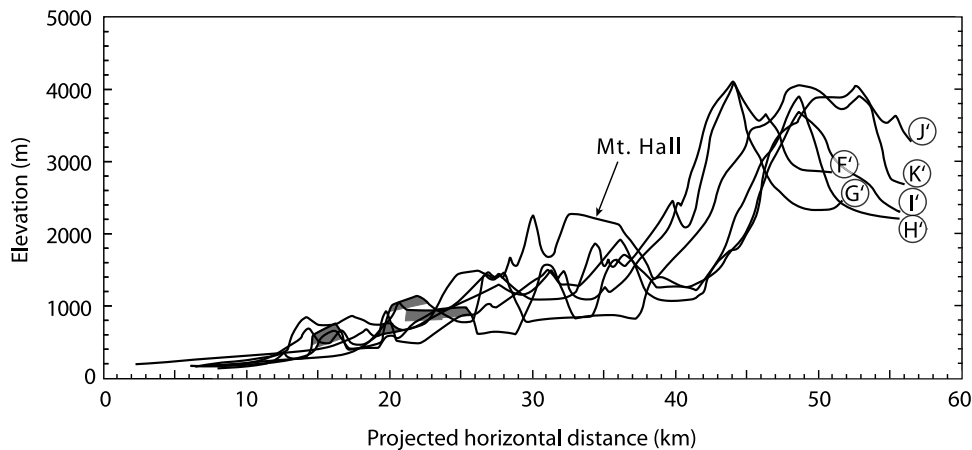


Figure 11. Topographic profiles of TAM front between Shackleton and Liv glaciers, oriented approximately perpendicular to the range and each spaced ~ 10 –25 km apart. Piedmont erosion surfaces are marked in gray. Exhumed Kukri erosion surface on Mount Hall is also visible. Vertical exaggeration is 5 \times . Projected onto vertical plane striking 027° (at 175°W), approximately perpendicular to the coastline. See Figure 9 for locations.

southeast of Cape Surprise, is exceptional, possibly indicating ~ 300 m vertical separation from adjacent surfaces in the along-strike direction, probably across range-perpendicular faults. Such faulting and block tilting is consistent with fault kinematic data for ESE directed ($\sim 100^\circ$) extension across NNE striking normal faults and may have given rise to

asymmetric drainage patterns in the TAM front [Miller et al., 2001].

6.6. Implications for Formation of the Transantarctic Mountains

[33] Thermochronology constrains cooling and hence denudation, but not directly rock uplift or surface uplift

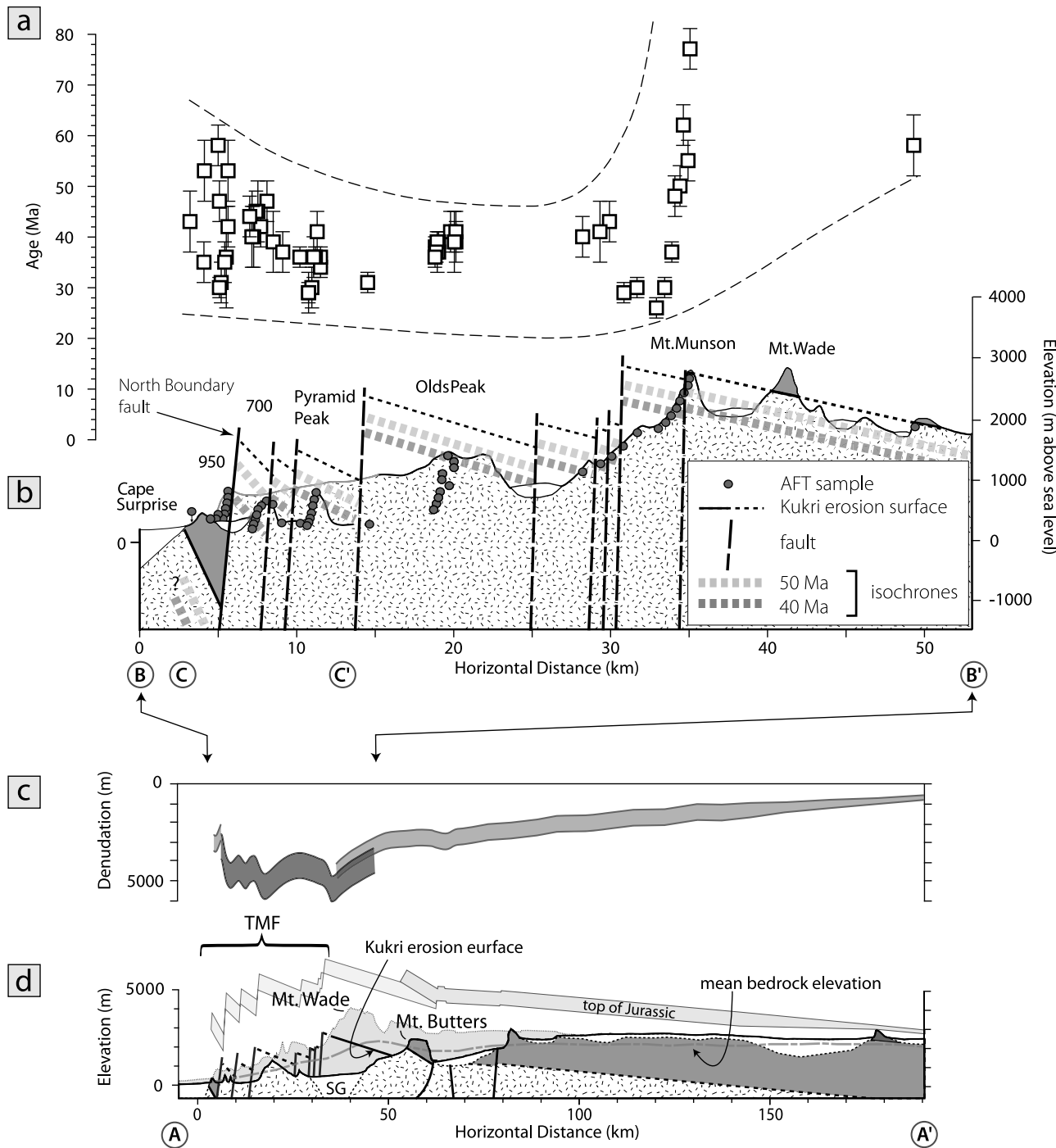


Figure 12

[e.g., *England and Molnar*, 1990]. Evidence suggests, however, that accelerated denudation in the Eocene was a direct response to tectonics within the TAM front. Cenozoic denudation in the Shackleton Glacier area, both in magnitude and location, is similar to elsewhere in the TAM, focused within the TAM front and coastward of the topographic crest. Rapid Cenozoic denudation in the Shackleton Glacier region began at ~ 40 Ma, generally later than in other segments of the TAM front but generally compatible with a previously noted trend that youngs southward along the range [*Fitzgerald*, 2002]. For instance, Cenozoic denudation began in northern Victoria Land at ~ 55 Ma [*Fitzgerald and Gleadow*, 1988]; southern Victoria Land at 55 Ma [*Gleadow and Fitzgerald*, 1987; *Fitzgerald*, 1992]; the Beardmore Glacier region at 50 Ma [*Fitzgerald*, 1994]; and the Scott Glacier region at ~ 45 Ma [*Fitzgerald and Stump*, 1997] (Figure 1b). As in the Shackleton Glacier area, Cenozoic denudation elsewhere in the TAM was associated with faulting across the TAM front. Vertically offset 30–35 Ma isochrones in both the Beardmore Glacier area [*Fitzgerald*, 1994] and near Granite Harbour in southern Victoria Land [*Fitzgerald*, 1992] show faulting in these areas probably continued to at least 30 Ma.

[34] Overall, these results have bearings on the proposed models for formation of the TAM, at least by providing observations that these and future models must incorporate. In the Shackleton Glacier area, normal faulting and denudation coincided with the 150–170 km of extension in the WARS between 43 and 26 Ma [*Cande et al.*, 2000; *Cande and Stock*, 2006; *Davey et al.*, 2006]. This supports the rift flank uplift model of the TAM, but does not explain the lack of coincidence between extension and denudation in other sectors of the range. Although there is evidence for dextral transtension and strike-slip motions between East and West Antarctica at this time [*Wilson*, 1995; *Müller et al.*, 2007], which has been suggested as a factor in Cenozoic uplift of the TAM [*ten Brink et al.*, 1997], NNE directed extension in the TAM front near the Shackleton Glacier suggests almost orthogonal extension [*Miller et al.*, 2001]. The demonstrated history of faulting in the TAM front is also inconsistent with

the hypothesis that most rock uplift in the TAM was Cretaceous and associated with wide rifting in the WARS, and that rapid denudation in the TAM front only began after climate became more conducive to erosion or after the WARS subsided below sea level [*Karner et al.*, 2005]. As we lack constraints on early Cenozoic land surface elevations, our results are consistent with both the hypothesis that the TAM are a Cenozoic rift flank uplift [*Fitzgerald et al.*, 1986; *Stern and ten Brink*, 1989; *van der Beek et al.*, 1994; *Busetti et al.*, 1999; *van Wyk et al.*, 2008] and the hypothesis that the TAM is a relict high-elevation margin of a collapsed continental plateau [*Bialas et al.*, 2007]. However, with respect to plateau collapse, our results indicate that any initial collapse and associated extension in the WARS (~ 105 –85 Ma) was not along the present-day TAM front. Any of the most recent extension observed within the WARS, such as in the Terror Rift [e.g., *Fielding et al.*, 2008], has not contributed to distributed faulting within the TAM front in the Shackleton Glacier region and is possibly only related to limited surface uplift. Finally, although glacial erosion may have been significant in the TAM and contributed to some isostatic uplift [*Stern et al.*, 2005], geomorphologic evidence in the TAM front suggests glacial erosion might have largely postdated most TAM front faulting. Based on the widespread occurrence of nonglacial landforms in the TAM [e.g., *Denton et al.*, 1993; *Jamieson and Sugden*, 2008], the role of fluvial or mixed fluvioglacial erosion may be greater than glacial erosion alone.

7. Conclusions

[35] The results of our study refine the history of faulting in the TAM front, linking it directly to Cenozoic denudation in the TAM front and extension in the WARS. Furthermore, our study demonstrates the utility of combining thermochronologic, geologic, and geomorphologic data in order to provide a complete picture of deformation and landscape evolution in an extensional mountain range. AFT thermochronology combined with stratigraphic constraints indicate that no significant normal faulting occurred across the TAM

Figure 12. Thermochronologic and structural summary diagram. (a) Central ages (squares) and errors ($\pm 2\sigma$) plotted above corresponding sample locations (circles) in Figure 12b. (b) Composite cross section of the TAM front, showing AFT sample locations, the 40 and 50 Ma isochrones, the projected Kukri erosion surface, and faults (dashed where inferred). The vertical distance of the Kukri erosion surface above the isochrones is known directly on Mount Munson and Mount Wade. Error (2σ) on elevation of isochrone at sample locations is approximately the thickness of the isochrone line. Possible faults near spot height 700 are not shown for clarity. Dip of the Kukri erosion surface is not well constrained between Mount Munson and Cape Surprise but is $\sim 3^\circ$ SW in the Prince Olav Mountains and $\sim 35^\circ$ SW at the coast [*Barrett*, 1965; *La Prade*, 1969]. Note that structural geometries are distorted by vertical exaggeration (4 \times). Cross sections B-B' and C-C' are located in Figure 3. Structures observed in C-C' do not necessarily project to B-B', particularly near Cape Surprise where mapped transfer faults occur between them. (c) Estimated Cenozoic denudation profile. See text for details. (d) Cross section of the TAM, from the East Antarctic Ice Sheet to the Ross Ice Shelf. Location is shown in Figure 1. Geology and observed faults are from *La Prade* [1969]; inferred faults are from cross section in Figure 12b. Only rift-parallel faults are shown (thick black lines). Gray silhouette in the background marks the envelope of maximum topographic elevations between Shackleton and Liv glaciers. Ice thickness based on the work by *Drewry* [1972]. The cross section crosses the Shackleton Glacier, SG, which overlies a suspected fault (not shown). Envelope indicating top of the Jurassic is based on regional stratigraphic measurements. Mean bedrock elevation (dashed gray line) is based on 50 km wide swath along A-A', extending from its east side, calculated from BEDMAP, which has a 5 km cell size [*Lythe et al.*, 2000]. Vertical exaggeration is 5 \times .

front on the east side of the Shackleton Glacier from the late Paleozoic to 40 Ma, despite Jurassic and Cretaceous extension within the adjacent WARS. This conclusion is based on the similar magnitudes of vertical offset of Beacon Supergroup strata down-faulted at Cape Surprise and cumulative offset on AFT isochrones. Mesozoic denudation was negligible. The vertically offset AFT isochrones show that extension is distributed across the TAM front by slip on multiple identifiable normal faults spaced over 20–30 km rather than on one master fault as previously proposed.

[36] Much of the presently exposed TAM front resided within an apatite PAZ until rapid denudation began near the Ross Ice Shelf coast at ~40 Ma, when denudation rates increased from <35 to 50–200 m/Myr, persisting until ~26 Ma. Denudation at Mount Munson, near the inland margin of the TAM front, began later at 30–35 Ma, indicating more distributed faulting in the TAM front or simply passive escarpment retreat. Since ~40 Ma there has been as much as 4.9–6.0 km of denudation over the TAM front.

[37] From <26 Ma to ~14 Ma a low-relief erosion surface formed across the TAM front. This erosion surface, since incised by the modern network of valley glaciers, is evident today in scattered relict surfaces. The lower limit of ~14 Ma for these erosion surfaces is based on similarities

with better dated landforms in southern Victoria Land and Marie Byrd Land. Erosion surfaces show no significant deformation across range-parallel faults in the TAM front and constrain most fault activity within the TAM front to the period of ~40–14 Ma. Since formation of the erosion surfaces, there has probably been minor throw on faults that strike perpendicular to the range and greater throw across one or more range-parallel faults near the margin of the Ross Ice Shelf. Slip along this inferred coastal fault or fault zone has resulted in no more than 370–790 m of rock and surface uplift in the TAM front since ~14 Ma. Further research on the chronology of late Cenozoic landscape evolution in the TAM, such as erosion surfaces, will advance our understanding of this mountain range's formation and its coupling with the adjacent rift system.

[38] **Acknowledgments.** We thank P. O'Sullivan for his contributions to generating AFT data while a research associate at Syracuse University, some of which are part of this paper. Graeme Dingle's assistance in the field was invaluable. We also thank Antarctic Support Associates, Helicopters New Zealand, Ken Borek Air, and U.S. Navy Squadron VXE-6 for logistical and field support. Comments from B. Wilkinson, D. Elliot, Associate Editor P. Kapp, and an anonymous reviewer improved the manuscript. This work was supported by U.S. National Science Foundation grant OPP93–16720.

References

- Ackert, R. P., Jr., and M. D. Kurz (2004), Age and uplift rates of Sirius Group sediments in the Dominion Range, Antarctica, from surface exposure dating and geomorphology, *Global Planet. Change*, **42**, 207–225, doi:10.1016/j.gloplacha.2004.02.001.
- Anderson, R. S., A. L. Densmore, and M. A. Ellis (1999), The generation and degradation of marine terraces, *Basin Res.*, **11**, 7–19, doi:10.1046/j.1365-2117.1999.00085.x.
- Ashworth, A. C., and G. Kuschel (2003), Fossil weevils (Coleoptera, Curculionidae) from latitude 85°S Antarctica, *Palaeogeogr. Palaeoclimatol. Palaeoecol.*, **191**, 191–202, doi:10.1016/S0031-0182(02)00712-5.
- Baldwin, S. L., P. G. Fitzgerald, B. Li, and S. R. Miller (1999), Thermal evolution of the Transantarctic Mountains in the Shackleton Glacier area, in *8th International Symposium on Antarctic Earth Sciences, Wellington, New Zealand, July 1999. Programme and Abstracts*, edited by D. N. B. Skinner, p. 212, R. Soc. of N. Z., Wellington.
- Balestrieri, M. L., G. Bigazzi, and C. Ghezzo (1997), Uplift-denudation of the Transantarctic Mountains between the David and the Mariner glaciers, northern Victoria Land (Antarctica): Constraints by apatite fission-track analysis, in *The Antarctic Region: Geological Evolution and Processes*, edited by C. A. Ricci, pp. 547–554, Terra Antart., Siena, Italy.
- Ballantyne, C. K., and M. P. Kirkbride (1987), Rockfall activity in upland Britain during the Loch Lomond stadial, *Geogr. J.*, **153**, 86–92, doi:10.2307/634474.
- Baroni, C., V. Noti, S. Ciccacci, G. Righini, and M. C. Salvatore (2005), Fluvial origin of the valley system in northern Victoria Land (Antarctica) from quantitative geomorphic analysis, *Geol. Soc. Am. Bull.*, **117**, 212–228, doi:10.1130/B25529.1.
- Barrett, P. J. (1965), Geology of the area between the Axel Heiberg and Shackleton Glaciers, Queen Maud Mountains, Antarctica, *N. Z. J. Geol. Geophys.*, **8**, 344–370.
- Barrett, P. J. (1981), History of the Ross Sea region during the deposition of the Beacon Supergroup 400–180 million years ago, *J. R. Soc. N. Z.*, **II**, 447–458.
- Barrett, P. J. (1991), The Devonian to Jurassic Beacon Supergroup of the Transantarctic Mountains and correlatives in other parts of Antarctica, in *The Geology of Antarctica*, edited by R. J. Tingey, pp. 120–152, Oxford Univ. Press, Oxford, U. K.
- Barrett, P. J., D. H. Elliot, and J. F. Lindsay (1986), The Beacon Supergroup (Devonian–Triassic) and Ferrar Group (Jurassic) in the Beardmore Glacier area, Antarctica, in *Geology of the Central Transantarctic Mountains, Antarct. Res. Ser.*, vol. 36, edited by M. D. Turner and J. F. Splettstoesser, pp. 339–428, AGU, Washington, D. C.
- Behrendt, J. C., and A. K. Cooper (1991), Evidence of rapid Cenozoic uplift of the shoulder escarpment of the West Antarctic rift system and a speculation on possible climate forcing, *Geology*, **19**, 315–318, doi:10.1130/0091-7613(1991)019<0315:EORCUO>2.3.CO;2.
- Benn, D. I., and D. J. A. Evans (1998), *Glaciers and glaciology*, Arnold, London.
- Bialas, R. W., W. R. Buck, M. Studinger, and P. G. Fitzgerald (2007), Plateau collapse model for the Transantarctic Mountains–West Antarctic rift system; insights from numerical experiments, *Geology*, **35**, 687–690, doi:10.1130/G23825A.1.
- Borg, S. G. (1983), Petrology and geochemistry of the Queen Maud Batholith, central Transantarctic Mountains, with implications for the Ross orogeny, in *Antarctic Earth Science—Fourth International Symposium*, edited by R. Oliver, P. James, and J. Jago, pp. 165–169, Cambridge Univ. Press, Cambridge, U. K.
- Borg, S. G., D. J. De Paulo, and B. M. Smith (1990), Isotopic structure and tectonics of the central Transantarctic Mountains, Antarctica, *Tectonophysics*, **200**, 1–16, doi:10.1016/0040-1907(90)90001-2.
- Braun, J. (2002), Quantifying the effect of recent relief changes on age-elevation relationships, *Earth Planet. Sci. Lett.*, **200**, 331–343, doi:10.1016/S0012-821X(02)00638-6.
- Brook, E. J., E. T. Brown, M. D. Kurz, R. P. Ackert, G. M. Raisbeck, and F. Yiou (1995), Constraints on age, erosion, and uplift of Neogene glacial deposits in the Transantarctic Mountains determined from *in situ* cosmogenic ^{10}Be and ^{26}Al , *Geology*, **23**, 1063–1066, doi:10.1130/0091-7613(1995)023<1063:COAEAU>2.3.CO;2.
- Burbank, D. W., and R. S. Anderson (2001), *Tectonic Geomorphology*, 274 pp., Blackwell Sci., Oxford, U. K.
- Burtner, R. L., A. Nigrini, and R. A. Donelick (1994), Thermochronology of Lower Cretaceous source rocks in the Idaho-Wyoming thrust belt, *AAPG Bull.*, **78**, 1613–1636.
- Busetti, M., G. Spadini, F. M. van der Wateren, S. A. P. L. Cloetingh, and C. Zanolla (1999), Kinematic modelling of the West Antarctic Rift system, Ross Sea, Antarctica, *Global Planet. Change*, **23**, 79–103, doi:10.1016/S0921-8181(99)00052-1.
- Cande, S. C., and J. M. Stock (2006), Constraints on the timing of extension in the Northern Basin, Ross Sea, in *Antarctica: Contributions to Global Earth Sciences*, edited by D. K. Fuetterer et al., pp. 319–326, Springer, Berlin.
- Cande, S. C., J. M. Stock, R. D. Mueller, and T. Ishihara (2000), Cenozoic motion between East and West Antarctica, *Nature*, **404**, 145–150, doi:10.1038/35004501.
- Carlson, W. D., R. A. Donelick, and R. A. Ketcham (1999), Variability of apatite fission-track annealing kinetics; I. Experimental results, *Am. Mineral.*, **84**, 1213–1233.
- Cole, K. L., and L. Mayer (1982), Use of packrat middens to determine rates of cliff retreat in the eastern Grand Canyon, Arizona, *Geology*, **10**, 597–599.

- doi:10.1130/0091-7613(1982)10<597:UOPMTD>2.0.CO;2.
- Collinson, J. W., and D. H. Elliot (1984), Triassic stratigraphy of the Shackleton Glacier Area, in *Geology of the Central Transantarctic Mountains, Antarctica*, Res. Ser., vol. 36, edited by M. D. Turner and J. F. Splettstoesser, pp. 103–117, AGU, Washington, D. C.
- Cooke, R. U., A. Warren, and A. Goudie (1993), *Desert Geomorphology*, 526 pp., UCL Press, London.
- Cooper, A. K., F. J. Davey, and K. Hinz (1991), Crustal extension and origin of sedimentary basins beneath the Ross Sea and Ross Ice Shelf, Antarctica, in *Geological Evolution of Antarctica*, edited by M. R. A. Thomson et al., pp. 285–291, Cambridge Univ. Press, New York.
- Davey, F. J., and G. Brancolini (1995), The late Mesozoic and Cenozoic structural setting of the Ross Sea region, in *Geology and Seismic Stratigraphy of the Antarctic Margin, Antarctica*, Res. Ser., vol. 68, edited by P. Barker and A. Cooper, pp. 167–182, AGU, Washington, D. C.
- Davey, F. J., S. C. Cande, and J. M. Stock (2006), Extension in the western Ross Sea region-links between Adare Basin and Victoria Land Basin, *Geophys. Res. Lett.*, 33, L20315, doi:10.1029/2006GL027383.
- Decesari, R. C., C. C. Sorlien, B. P. Luyendyk, D. S. Wilson, L. Bartek, J. Diebold, and S. E. Hopkins (2007a), Regional seismic stratigraphic correlations of the Ross Sea: implications for the tectonic history of the West Antarctic Rift System, in *Antarctica: A Keystone in a Changing World—Online Proceedings of the 10th ISAES*, edited by A. K. Cooper and C. R. Raymond, U.S. Geol. Surv. Open File Rep., 2007-1047, SRP 052, doi:10.3133/of2007-1047.srp052.
- Decesari, R. C., D. S. Wilson, B. P. Luyendyk, and M. Faulkner (2007b), Cretaceous and Tertiary extension throughout the Ross Sea, Antarctica, in *Antarctica: A Keystone in a Changing World—Online Proceedings for the 10th International Symposium on Antarctic Earth Sciences, Santa Barbara, California, U.S.A.—August 26 to September 1, 2007*, edited by A. Cooper, C. Raymond, and the 10th ISAES Editorial Team, U.S. Geol. Surv. Open File Rep., 2007-1047, SRP 098, doi:10.3133/of2007-1047.srp098.
- Denton, G. H., D. E. Sugden, D. R. Marchant, B. L. Hall, and T. I. Wilch (1993), East Antarctic Ice Sheet sensitivity to Pliocene climatic change from a Dry Valleys perspective, *Geogr. Ann.*, 75, 155–204, doi:10.2307/521200.
- DiVenere, V. J., D. V. Kent, and I. W. D. Dalziel (1994), Mid-Cretaceous paleomagnetic results from Marie Byrd Land, West Antarctica: A test of post-100 Ma relative motion between East and West Antarctica, *J. Geophys. Res.*, 99, 15,115–15,139, doi:10.1029/94JB00807.
- Di Vincenzo, G., S. Rocchi, F. Rossetti, and F. Storti (2004), ^{40}Ar - ^{39}Ar dating of pseudotachylites; the effect of clast-hosted extraneous argon in Cenozoic fault-generated friction melts from the West Antarctic rift system, *Earth Planet. Sci. Lett.*, 223, 349–364, doi:10.1016/j.epsl.2004.04.042.
- Donelick, R. A., R. A. Ketchem, and W. D. Carlson (1999), Variability of apatite fission-track annealing kinetics; II, Crystallographic orientation effects, *Am. Mineral.*, 84, 1224–1234.
- Drewry, D. J. (1972), The contribution of radio echo sounding to the investigation of Cenozoic tectonics and glaciation in Antarctica, in *Polar Geomorphology*, edited by C. J. Price and D. E. Sugden, Spec. Publ. 4, pp. 43–58, Inst. of Br. Geogr., London.
- Dumitru, T. A. (1993), A new computer-automated microscope stage system for fission-track analysis, *Nucl. Tracks Radiat. Meas.*, 21, 575–580, doi:10.1016/1359-0189(93)90198-1.
- Elliot, D. H. (1992), Continental break-up, magmatism, and tectonism: An Antarctic perspective, in *Migmatism and the Causes of Continental Break-up*, edited by B. C. Storey et al., *Geol. Soc. Spec. Publ.*, 68, 165–184.
- Elliot, D. H., and T. H. Fleming (2004), Occurrence and dispersal of magmas in the Jurassic Ferrar large igneous province, Antarctica, *Gondwana Res.*, 7, 223–237, doi:10.1016/S1342-937X(05)70322-1.
- Elliot, D. H., and D. Larsen (1993), Mesozoic volcanism in the Transantarctic Mountains: Depositional environment and tectonic setting, in *Gondwana 8: Assembly, Evolution, and Dispersal*, edited by R. H. Findlay et al., pp. 397–414, A. A. Balkema, Rotterdam, Netherlands.
- England, P. C., and P. Molnar (1990), Surface uplift, uplift of rocks, and exhumation of rocks, *Geology*, 18, 1173–1177, doi:10.1130/0091-7613(1990)018<1173:SUUORA>2.3.CO;2.
- Fielding, C. R., J. Whittaker, S. A. Henrys, T. J. Wilson, and T. R. Naish (2008), Seismic facies and stratigraphy of the Cenozoic succession in McMurdo Sound, Antarctica; implications for tectonic, climatic and glacial history, *Palaeogeogr. Palaeoclimatol. Palaeoecol.*, 260, 8–29, doi:10.1016/j.palaeo.2007.08.016.
- Fitzgerald, P. G. (1992), The Transantarctic Mountains of southern Victoria Land: The application of apatite fission track analysis to a rift shoulder uplift, *Tectonics*, 11, 634–662, doi:10.1029/91TC02495.
- Fitzgerald, P. G. (1994), Thermochronologic constraints on post-Paleozoic tectonic evolution of the central Transantarctic Mountains, Antarctica, *Tectonics*, 13, 818–836, doi:10.1029/94TC00595.
- Fitzgerald, P. G. (2002), Tectonics and landscape evolution of the Antarctic Plate since the breakup of Gondwana, with an emphasis on the West Antarctic rift system and the Transantarctic Mountains, *Bull. R. Soc. N. Z.*, 35, 453–469.
- Fitzgerald, P. G., and S. Baldwin (1997), Detachment fault model for the evolution of the Ross embayment, in *The Antarctic Region: Geological Evolution and Processes*, edited by C. Ricci, pp. 555–564, Terra Antarct., Siena, Italy.
- Fitzgerald, P. G., and S. L. Baldwin (2007), Thermochronologic constraints on Jurassic rift flank denudation in the Thiel Mountains, Antarctica, in *Antarctica: A Keystone in a Changing World—Online Proceedings for the 10th International Symposium on Antarctic Earth Sciences, Santa Barbara, California, U.S.A.—August 26 to September 1, 2007*, edited by A. Cooper, C. Raymond, and the 10th ISAES Editorial Team, U.S. Geol. Surv. Open File Rep., 2007-1047, SRP 098, doi:10.3133/of2007-1047.srp098.
- Fitzgerald, P. G., and A. J. W. Gleadow (1988), Fission-track geochronology, tectonics and structure of the Transantarctic Mountains in northern Victoria Land, Antarctica, *Chem. Geol.*, 73, 169–198.
- Fitzgerald, P. G., and A. J. W. Gleadow (1990), New approaches in fission track geochronology as a tectonic tool: Examples from the Transantarctic Mountains, *Nucl. Tracks Radiat. Meas.*, 17, 351–357, doi:10.1016/1359-0189(90)90057-5.
- Fitzgerald, P. G., and E. Stump (1997), Cretaceous and Cenozoic episodic denudation of the Transantarctic Mountains, Antarctica: New constraints from apatite fission track thermochronology in the Scott Glacier region, *J. Geophys. Res.*, 102, 7747–7765, doi:10.1029/96JB03898.
- Fitzgerald, P. G., M. Sandiford, P. J. Barrett, and A. J. W. Gleadow (1986), Asymmetric extension associated with uplift and subsidence of the Transantarctic Mountains and Ross Embayment, *Earth Planet. Sci. Lett.*, 81, 67–78, doi:10.1016/0012-821X(86)90101-9.
- Fitzgerald, P. G., S. L. Baldwin, L. E. Webb, and P. O'Sullivan (2006), Interpretation of (U-Th)/He single grain ages from slowly cooled crustal terranes; a case study from the Transantarctic Mountains of southern Victoria Land, *Chem. Geol.*, 225, 91–120, doi:10.1016/j.chemgeo.2005.09.001.
- Foster, D. A., and A. J. W. Gleadow (1996), Structural framework and denudation history of the flanks of the Kenya and Anza rifts, East Africa, *Tectonics*, 15, 258–271, doi:10.1029/95TC02744.
- Galbraith, R. F., and G. M. Laslett (1993), Statistical models for mixed fission track ages, *Nucl. Tracks Radiat. Meas.*, 21, 459–470, doi:10.1016/1359-0189(93)90185-C.
- Gallagher, K., C. J. Hawkesworth, and M. S. M. Mantovani (1995), Denudation, fission track analysis and the long-term evolution of passive margin topography: Application to the southeast Brazilian margin, *J. South Am. Earth Sci.*, 8, 65–77, doi:10.1016/0895-9811(94)00042-Z.
- Gallagher, K., R. Brown, and C. Johnson (1998), Fission track analysis and its applications to geological problems, *Annu. Rev. Earth Planet. Sci.*, 26, 519–572, doi:10.1146/annurev.earth.26.1.519.
- Gilchrist, A. R., and M. A. Summerfield (1990), Differential denudation and flexural isostasy in the formation of rifted-margin upwarps, *Nature*, 346, 739–742, doi:10.1038/346739a0.
- Gleadow, A. J. W. (1981), Fission-track dating methods: what are the real alternatives?, *Nucl. Tracks*, 5, 3–14, doi:10.1016/0191-278X(81)90021-4.
- Gleadow, A. J. W., and P. G. Fitzgerald (1987), Uplift history and structure of the Transantarctic Mountains: New evidence from fission track dating of basement apatites in the Dry Valleys area, southern Victoria Land, *Earth Planet. Sci. Lett.*, 82, 1–14, doi:10.1016/0012-821X(87)90102-6.
- Goodge, J. W., P. Myrow, D. Phillips, C. M. Fanning, and I. S. Williams (2004a), Siliciclastic record of rapid denudation in response to convergent-margin orogenesis, Ross Orogen, Antarctica, in *Detrital Thermochronology—Provenance Analysis, Exhumation, and Landscape Evolution of Mountain Belts*, edited by M. Bernet and C. Spiegel, *Spec. Pap. Geol. Soc. Am.*, 378, 105–126.
- Goodge, J. W., I. S. Williams, and P. Myrow (2004b), Provenance of Neoproterozoic and lower Paleozoic siliciclastic rocks of the central Ross Orogen, Antarctica; detrital record of rift-, passive-, and active-margin sedimentation, *Geol. Soc. Am. Bull.*, 116, 1253–1279, doi:10.1130/B25347.1.
- Gunn, B. M., and G. Warren (1962), Geology of Victoria Land between the Mawson and Mulock glaciers, Antarctica, *N. Z. Geol. Surv. Bull.*, 71, 157 pp.
- Hall, S. R., D. L. Farber, L. Audin, R. C. Finkel, and A. S. Meriaux (2008), Geochronology of pediment surfaces in southern Peru; implications for Quaternary deformation of the Andean fore-arc, *Tectonophysics*, 459, 186–205, doi:10.1016/j.tecto.2007.11.073.
- Hambrey, M. J., P.-N. Webb, D. M. Harwood, and L. A. Krissek (2003), Neogene glacial record from the Sirius Group of the Shackleton Glacier region, central Transantarctic Mountains, Antarctica, *Geol. Soc. Am. Bull.*, 115, 994–1015, doi:10.1130/B25183.1.
- Hamilton, W., P. T. Hayes, R. Calvert, V. C. Smith, P. S. D. Elmore, P. R. Barnett, and N. Conklin (1965), Diabase sheets of the Taylor Glacier region, Victoria Land, Antarctica, *U.S. Geol. Surv. Prof. Pap.*, 456B.
- Haq, B. U., and A. M. Al-Qahtani (2005), Phanerozoic cycles of sea-level change on the Arabian Platform, *GeoArabia*, 10, 127–160.
- Haq, B. U., L. A. Hardenbol, and P. R. Vail (1987), Chronology of fluctuating sea levels since the Triassic, *Science*, 235, 1156–1167, doi:10.1126/science.235.4793.1156.
- Hurford, A. J., and P. F. Green (1983), The zeta age calibration of fission-track dating, *Ios. Geosci.*, 1, 285–317.
- Huybrechts, P. (1993), Glaciological modelling of the late Cenozoic East Antarctic ice sheet; stability or dynamism?, *Geogr. Ann.*, 75, 221–238, doi:10.2307/521202.
- Isbell, J. L. (1999), The Kukri erosion surface; a reassessment of its relationship to rocks of the Beacon Supergroup in the central Transantarctic Mountains, Antarctica, *Antarct. Sci.*, 11, 228–238, doi:10.1017/S0954102099000292.
- Jamieson, S. S. R., and D. E. Sugden (2008), Landscape Evolution of Antarctica, in *Antarctica: A*

- Keystone in a Changing World*, edited by A. K. Cooper et al., pp. 39–54, Natl. Acad. Press, Washington, D. C.
- Jamieson, S. S. R., N. R. J. Hulton, D. E. Sugden, A. J. Payne, and J. Taylor (2005), Cenozoic landscape evolution of the Lambert Basin, East Antarctica; the relative role of rivers and ice sheets, *Global Planet. Change*, **45**, 35–49, doi:10.1016/j.gloplacha.2004.09.015.
- Jones, S. (1997), Late Quaternary faulting and neotectonics, South Victoria Land, Antarctica, *J. Geol. Soc.*, **154**, 645–652, doi:10.1144/gsjgs.154.4.0645.
- Karner, G. D., M. Studinger, and R. E. Bell (2005), Gravity anomalies of sedimentary basins and their mechanical implications: Application to the Ross Sea basins, West Antarctica, *Earth Planet. Sci. Lett.*, **235**, 577–596, doi:10.1016/j.epsl.2005.04.016.
- Katz, H. R. (1982), Post-Beacon tectonics in the region of Amundsen and Scott glaciers, Queen Maud Range, Transantarctic Mountains, in *Antarctic Geoscience*, edited by C. Craddock, pp. 827–834, Univ. of Wisconsin Press, Madison.
- Kerr, A., and P. Huybrechts (1999), The response of the East Antarctic ice-sheet to the evolving tectonic configuration of the Transantarctic Mountains, *Global Planet. Change*, **23**, 213–229, doi:10.1016/S0921-8181(99)00058-2.
- Ketcham, R. A., R. A. Donelick, and W. D. Carlson (1999), Variability of apatite fission track annealing kinetics III: Extrapolation to geological time scales, *Am. Mineral.*, **84**, 1235–1255.
- Ketcham, R. A., R. A. Donelick, and M. B. Donelick (2000), AFTSolve: A program for multi-kinetic modeling of apatite fission-track data, *Geol. Mater. Res.*, **2**, 1–32.
- Komlinz, M. A. (1984), Oceanic ridge volumes and sea level change: An error analysis, in *Interregional Unconformities and Hydrocarbon Accumulation*, edited by J. S. Schlee, AAPG Mem., **36**, 109–127.
- Komlinz, M. A., K. G. Miller, and J. V. Browning (1998), Long-term and short-term global Cenozoic sea-level estimates, *Geology*, **26**, 311–314, doi:10.1130/0091-7613(1998)026-0311:LTASTG>2.3.CO;2.
- Kurz, M. D., and R. P. Ackert (1997), Stability of the East Antarctic Ice Sheet?: New chronological evidence from Bennett Platform, Antarctica, *Eos Trans. AGU*, **78**(17), Spring Meet. Suppl., **78**, S185.
- Laird, M. G. (1963), Geomorphology and stratigraphy of the Nimrod Glacier–Beaumont Bay region, southern Victoria Land, Antarctica, *N. Z. J. Geol. Geophys.*, **6**, 465–484.
- La Prade, K. E. (1969), Geology of Shackleton Glacier area, Queen Maud Range, Transantarctic Mountains, Antarctica, Ph.D. thesis, Tex. Technol. Coll., Lubbock.
- La Prade, K. E. (1970), Permian-Triassic Beacon group of the Shackleton glacier area, Queen Maud range, Transantarctic mountains, Antarctica, *Geol. Soc. Am. Bull.*, **81**, 1403–1410, doi:10.1130/0016-7606(1970)81[1403:PBGOTS]2.0.CO;2.
- Laslett, G. M., W. S. Kendall, A. J. W. Gleadow, and I. R. Duddy (1982), Bias in measurement of fission-track length distributions, *Nucl. Tracks Radiat. Meas.*, **6**, 79–85, doi:10.1016/0735-245X(82)90031-X.
- Laslett, G. M., A. J. W. Gleadow, and I. R. Duddy (1984), The relationship between fission track length and density in apatite, *Nucl. Tracks Radiat. Meas.*, **9**, 29–38, doi:10.1016/0735-245X(84)90019-X.
- Lawver, L. A., and L. M. Gahagan (1994), Constraints on timing of extension in the Ross Sea region, *Terra Antarct.*, **1**, 545–552.
- Lawver, L. A., and L. M. Gahagan (1995), Revised plate reconstructions and implications for extension in the Ross Sea region, paper presented at VII International Symposium on Antarctic Earth Sciences, Sci. Comm. on Antarct. Res., Siena, Italy, 10–15 Sept.
- LeMasurier, W. E., and C. A. Landis (1996), Mantle-plume activity recorded by low-relief erosion surfaces in West Antarctica and New Zealand, *Geol. Soc. Am. Bull.*, **108**, 1450–1466, doi:10.1130/0016-7606(1996)108<1450:MPARBL>2.3.CO;2.
- Lewis, A. R., D. R. Marchant, D. E. Kowalewski, S. L. Baldwin, and L. E. Webb (2006), The age and origin of the Labyrinth, western Dry Valleys, Antarctica: Evidence for extensive middle Miocene subglacial floods and freshwater discharge to the Southern Ocean, *Geology*, **34**, 513–516, doi:10.1130/G22145.1.
- Lewis, A. R., D. R. Marchant, A. C. Ashworth, S. R. Hemming, and M. L. Machlus (2007), Major middle Miocene global climate change: evidence from East Antarctica and the Transantarctic Mountains, *Geol. Soc. Am. Bull.*, **119**, 1449–1461, doi:10.1130/B26134.
- Lisker, F. (2002), Review of fission track studies in northern Victoria Land, Antarctica; passive margin evolution versus uplift of the Transantarctic Mountains, *Tectonophysics*, **349**, 57–73, doi:10.1016/S0040-1951(02)00046-X.
- Lisker, F., A. L. Laeuffer, M. Olesch, F. Rossetti, and T. Schaefer (2006), Transantarctic Basin; new insights from fission-track and structural data from the USARP Mountains and adjacent areas (northern Victoria Land, Antarctica), *Basin Res.*, **18**, 497–520, doi:10.1111/j.1365-2117.2006.00301.x.
- Liu, H., K. Jezek, B. Li, and Z. Zhao (2001), Radarsat Antarctic Mapping Project digital elevation model version 2, Natl. Snow and Ice Data Cent., Boulder, Colo.
- Luyendyk, B. P., C. C. Sorlien, D. S. Wilson, L. R. Bartek, and C. S. Siddoway (2001), Structural and tectonic evolution of the Ross Sea Rift in the Cape Colbeck region, eastern Ross Sea, Antarctica, *Tectonics*, **20**, 933–958, doi:10.1029/2000TC001260.
- Luyendyk, B. P., D. S. Wilson, and C. S. Siddoway (2003), Eastern margin of the Ross Sea Rift in western Marie Byrd Land, Antarctica: Crustal structure and tectonic development, *Geochem. Geophys. Geosyst.*, **4**(10), 1090, doi:10.1029/2002GC000462.
- Lythe, M. B., D. G. Vaughan, and B. Consortium (2000), BEDMAP—Bed topography of the Antarctic, 1:10,000,000 scale map, BAS (Misc) 9, Br. Antarct. Surv., Cambridge, U. K.
- Mancktelow, N. S., and B. Grasemann (1997), Time-dependent effects of heat advection and topography on cooling histories during erosion, *Tectonophysics*, **270**, 167–195, doi:10.1016/S0040-1951(96)00279-X.
- Marchant, D. R., G. H. Denton, C. C. Swisher III, and N. Potter Jr. (1996), Late Cenozoic Antarctic paleoclimate reconstructed from volcanic ashes in the Dry Valleys region of southern Victoria Land, *Geol. Soc. Am. Bull.*, **108**, 181–194, doi:10.1130/0016-7606(1996)108<0181:LCAPRF>2.3.CO;2.
- McGregor, V. R. (1965), Geology of the area between the Axel Heiberg and Shackleton Glaciers, Queen Maud Range, Antarctica. Part I—Basement complex, structure, and glacial geology, *N. Z. J. Geol. Geophys.*, **8**, 314–343.
- McGregor, V. R., and F. A. Wade (1969), Geology of the western Queen Maud Mountains, Geologic Map of Antarctica, Sheet 16, Am. Geogr. Soc., New York.
- Miller, K. G., et al. (2005), The Phanerozoic record of global sea-level change, *Science*, **310**, 1293–1298, doi:10.1126/science.1116412.
- Miller, S. R., P. G. Fitzgerald, and S. L. Baldwin (2001), Structure and kinematics of the central Transantarctic Mountains; constraints from structural geology and geomorphology near Cape Surprise, *Terra Antarct.*, **8**, 11–24.
- Mortimer, N., P. J. Forsyth, and I. M. Turnbull (2002), Reassessment of faults in the Wilson Piedmont Glacier area: Implications for age and style of Transantarctic Mountains uplift, in *Antarctica at the Close of a Millennium*, edited by J. A. Gamble et al., pp. 207–213, R. Soc. of N. Z., Wellington.
- Mortimer, N., W. J. Dunlap, M. J. Isaac, R. P. Sutherland, and K. Faure (2007), Basal Adare Volcanics, Robertson Bay, north Victoria Land, Antarctica; late Miocene intraplate basalts of subaqueous origin, in *Antarctica: A Keystone in a Changing World—Online Proceedings for the 10th International Symposium on Antarctic Earth Sciences, Santa Barbara, California, U.S.A.—August 26 to September 1, 2007*, edited by A. Cooper, C. Raymond, and the 10th ISAES Editorial Team, U.S. Geol. Surv. Open File Rep., 2007-1047, SRP 045, doi:10.3133/of2007-1047.srp045.
- Müller, R. D., K. Gohl, S. C. Candé, A. Goncharov, and A. V. Golynsky (2007), Eocene to Miocene geometry of the West Antarctic Rift system, *Aust. J. Earth Sci.*, **54**, 1033–1045, doi:10.1080/08120090701615691.
- Naish, T. R., et al. (2001), Orbitally induced oscillations in the East Antarctic ice sheet at the Oligocene/Miocene boundary, *Nature*, **413**, 719–723, doi:10.1038/35099534.
- Passchier, S. (2004), Variability in geochemical provenance and weathering history of Sirius Group strata, Transantarctic Mountains; implications for Antarctic glacial history, *J. Sediment. Res.*, **74**, 607–619, doi:10.1306/022704740607.
- Paulsen, T. S., J. Encarnacion, and A. M. Grunow (2004), Structure and timing of transpressional deformation in the Shackleton Glacier area, Ross Orogen, Antarctica, *J. Geol. Soc.*, **161**, 1027–1038, doi:10.1144/0016-764903-040.
- Priesnitz, K. (1988), Cryoplanation, in *Advances in Periglacial Geomorphology*, edited by M. J. Clark, pp. 49–67, John Wiley, Chichester, U. K.
- Redfield, T. F. (1994), The Transantarctic Mountains of northern Victoria Land: Underplating, episodic uplift, and flexural suppression, Ph.D. thesis, Ariz. State Univ., Tempe.
- Reiners, P. W., Z. Zhou, T. A. Ehlers, X. Changhai, M. T. Brandon, R. A. Donelick, and S. Nicolescu (2003), Post-orogenic evolution of the Dabie Shan, eastern China, from (U-Th)/He and fission track thermochronology, *Am. J. Sci.*, **303**, 489–518, doi:10.2475/ajs.303.6.489.
- Rocchi, S., W. E. LeMasurier, and G. Di Vincenzo (2006), Oligocene to Holocene erosion and glacial history in Marie Byrd Land, West Antarctica, inferred from exhumation of the Dorrel Rock intrusive complex and from volcano morphologies, *Geol. Soc. Am. Bull.*, **118**, 991–1005, doi:10.1130/B25675.1.
- Rossetti, F., F. Lisker, F. Storti, and A. L. Läufer (2003), Tectonic and denudational history of the Rennick Graben (North Victoria Land): Implications for the evolution of rifting between East and West Antarctica, *Tectonics*, **22**(2), 1016, doi:10.1029/2002TC001416.
- Rossetti, F., F. Storti, M. Busetti, F. Lisker, G. Di Vincenzo, A. L. Läufer, S. Rocchi, and F. Salvini (2006), Eocene initiation of Ross Sea dextral faulting and implications for East Antarctic neotectonics, *J. Geol. Soc.*, **163**, 119–126, doi:10.1144/0016-764905-005.
- Schmidt, K.-H. (1988), Rates of scarp retreat: A means of dating Neotectonic activity, in *The Atlas System of Morocco*, edited by V. H. Jacobshagen, pp. 445–462, Springer, Berlin.
- Schmidt, K.-H. (1989), The significance of scarp retreat for Cenozoic landform evolution on the Colorado Plateau, USA, *Earth Surf. Processes Landforms*, **14**, 93–105, doi:10.1002/esp.3290140202.
- Siddoway, C. S., S. L. Baldwin, P. G. Fitzgerald, C. M. Fanning, and B. P. Luyendyk (2004), Ross Sea mylonites and the timing of intracontinental extension within the West Antarctic rift system, *Geology*, **32**, 57–60, doi:10.1130/G20005.1.
- Spasojević, S., L. Liu, M. Gurnis, and R. D. Müller (2008), The case for dynamic subsidence of the U.S. east coast since the Eocene, *Geophys. Res. Lett.*, **35**, L08305, doi:10.1029/2008GL033511.
- Steckler, M. S., and G. I. Omar (1994), Controls on erosional retreat of the uplifted rift flanks at the Gulf of Suez and northern Red Sea, *J. Geophys. Res.*, **99**, 12,159–12,173, doi:10.1029/94JB00278.

- Stern, T. A., and U. S. ten Brink (1989), Flexural uplift of the Transantarctic Mountains, *J. Geophys. Res.*, **94**, 10,315–10,330, doi:10.1029/JB094iB08p10315.
- Stern, T. A., A. K. Baxter, and P. J. Barrett (2005), Isostatic rebound due to glacial erosion within the Transantarctic Mountains, *Geology*, **33**, 221–224, doi:10.1130/G21068.1.
- Storti, F., M. L. Balestrieri, F. Balsamo, and F. Rossetti (2008), Structural and thermochronological constraints on the evolution of the West Antarctic Rift System in central Victoria Land, *Tectonics*, **27**, TC4012, doi:10.1029/2006TC002066.
- Studinger, M., R. E. Bell, W. R. Buck, G. D. Karner, and D. D. Blankenship (2004), Sub-ice geology of the Transantarctic Mountains in light of new aerogeophysical data, *Earth Planet. Sci. Lett.*, **220**, 391–408, doi:10.1016/S0012-821X(04)00066-4.
- Stump, E. (1995), *The Ross Orogen of the Transantarctic Mountains*, 284 pp., Cambridge Univ. Press, Cambridge, U. K.
- Stump, E., and P. G. Fitzgerald (1992), Episodic uplift of the Transantarctic Mountains, *Geology*, **20**, 161–164, doi:10.1130/0091-7613(1992)020<0161:EUOTTM>2.3.CO;2.
- Stüwe, K., L. White, and R. Brown (1994), The influence of eroding topography on steady-state isotherms. Application to fission track analysis, *Earth Planet. Sci. Lett.*, **124**, 63–74, doi:10.1016/0012-821X(94)00068-9.
- Sugden, D., and G. Denton (2004), Cenozoic landscape evolution of the Convoy Range to Mackay Glacier area, Transantarctic Mountains; onshore to offshore synthesis, *Geol. Soc. Am. Bull.*, **116**, 840–857, doi:10.1130/B25356.1.
- Sugden, D. E., G. H. Denton, and D. R. Marchant (1995), Landscape evolution of the Dry Valleys, Transantarctic Mountains; tectonic implications, *J. Geophys. Res.*, **100**, 9949–9967, doi:10.1029/94JB02875.
- Summerfield, M. A., F. M. Stuart, H. A. P. Cockburn, D. E. Sugden, G. H. Denton, T. Dunai, and D. R. Marchant (1999), Long-term rates of denudation in the Dry Valleys, Transantarctic Mountains, southern Victoria Land, Antarctica based on in-situ-produced cosmogenic ^{21}Ne , *Geomorphology*, **27**, 113–129, doi:10.1016/S0169-555X(98)00093-2.
- ten Brink, U. S., R. I. Hackney, S. Bannister, T. A. Stern, and Y. Makovsky (1997), Uplift of the Transantarctic Mountains and the bedrock beneath the East Antarctic ice sheet, *J. Geophys. Res.*, **102**, 27,603–27,621, doi:10.1029/97JB02483.
- van der Beek, P., S. Cloetingh, and P. Andriessen (1994), Mechanisms of extensional basin formation and vertical motions at rift flanks: Constraints from tectonic modelling and fission-track thermochronology, *Earth Planet. Sci. Lett.*, **121**, 417–433, doi:10.1016/0012-821X(94)90081-7.
- van der Wateren, F. M., A. L. L. M. Verbers, B. P. Luyendyk, and C. H. Smith (1996), Constraints on late Cenozoic rift shoulder uplift from landscape evolution studies in the Ross Sea area, in *Geodynamic Evolution of the Transantarctic Mountains and the West Antarctic Rift System: Proceedings of a Workshop*, edited by T. J. Wilson and C. A. Finn, *BPRC Rep.* **9**, pp. 40–43, Byrd Polar Res. Cent., Ohio State Univ., Columbus.
- Van Sickel, W. A., M. A. Kominz, K. G. Miller, and J. V. Browning (2004), Late Cretaceous and Cenozoic sea-level estimates: Backstripping analysis of borehole data, onshore New Jersey, *Basin Res.*, **16**, 451–465, doi:10.1111/j.1365-2117.2004.00242.x.
- van Wijk, J. W., J. F. Lawrence, and N. W. Driscoll (2008), Formation of the Transantarctic Mountains related to extension of the West Antarctic Rift system, *Tectonophysics*, **458**, 117–126, doi:10.1016/j.tecto.2008.03.009.
- Webb, P.-N., D. M. Harwood, B. C. McKelvey, M. G. C. Mabin, and J. H. Mercer (1986), Late Cenozoic tectonic and glacial history of the Transantarctic Mountains, *Antarct. J. U. S.*, **21**, 99–100.
- Webb, P.-N., D. M. Harwood, M. G. C. Mabin, and B. C. McKelvey (1996), A marine and terrestrial Sirius Group succession, middle Beardmore Glacier–Queen Alexandra Range, Transantarctic Mountains, Antarctica, *Mar. Micropaleontol.*, **27**, 273–297, doi:10.1016/0377-8398(95)00066-6.
- Weissel, J. K., and M. A. Seidl (1997), Influence of rock strength properties on escarpment retreat across passive continental margins, *Geology*, **25**, 631–634, doi:10.1130/0091-7613(1997)025<0631:IORSP>2.3.CO;2.
- Wilch, T. I., D. R. Lux, G. H. Denton, and W. C. McIntosh (1993), Minimal Pliocene-Pleistocene uplift of the dry valleys sector of the Transantarctic Mountains: A key parameter in ice-sheet reconstructions, *Geology*, **21**, 841–844, doi:10.1130/0091-7613(1993)021<0841:MPPUOT>2.3.CO;2.
- Wilson, D. S., and B. P. Luyendyk (2006), Bedrock platforms within the Ross Embayment, West Antarctica; hypotheses for ice sheet history, wave erosion, Cenozoic extension, and thermal subsidence, *Geochem. Geophys. Geosyst.*, **7**, Q12011, doi:10.1029/2006GC001294.
- Wilson, G. S., D. M. Harwood, R. A. Askin, and R. H. Levy (1998), Late Neogene Sirius Group strata in Reedy Valley, Antarctica: A multiple-resolution record of climate, ice-sheet and sea-level events, *J. Glaciol.*, **44**, 437–447.
- Wilson, T. J. (1992), Mesozoic and Cenozoic kinematic evolution of the Transantarctic mountains, in *Recent Progress in Antarctic Earth Science*, edited by Y. Yoshida et al., pp. 303–314, Terra Sci., Tokyo.
- Wilson, T. J. (1993), Jurassic faulting and magmatism in the Transantarctic Mountains: Implications for Gondwana break-up, in *Gondwana Eight—Assembly, evolution, and dispersal*, edited by R. H. Findlay et al., pp. 563–572, A. A. Balkema, Rotterdam, Netherlands.
- Wilson, T. J. (1995), Cenozoic transtension along the Transantarctic Mountains-West Antarctic rift boundary, southern Victoria Land, Antarctica, *Tectonics*, **14**, 531–545, doi:10.1029/94TC02441.
- Wrenn, J. H., and P.-N. Webb (1982), Physiographic analysis and interpretation of the Ferrar Glacier–Victoria Valley area, Antarctica, in *Antarctic Geoscience*, edited by C. Craddock, pp. 1091–1099, Univ. of Wis. Press, Madison.

S. L. Baldwin, P. G. Fitzgerald, and S. R. Miller,
Department of Earth Sciences, Syracuse University,
Syracuse, NY 13244, USA. (srmill02@syr.edu)